AGU PUBLICATIONS

Water Resources Research

RESEARCH ARTICLE
10.1002/2015WR018097

Key Points:
- We model the connectivity of multiple sediment cascades at the whole river network scale
- We identify all sediment source-sink relations to quantify all domains of sediment connectivity
- Sediment supply and local hydro-morphology control emerging patterns of connectivity

Supporting Information:
- Supporting Information S1
- Movie S1

Correspondence to:
R. J. P. Schmitt,
rafaeljan.schmitt@polimi.it

Citation:
Schmitt, R. J. P., S. Bizzi, and A. Castelletti (2016), Tracking multiple sediment cascades at the river network scale identifies controls and emerging patterns of sediment connectivity, *Water Resour. Res.*, *52*, 3941–3965, doi:10.1002/2015WR018097.

Received 10 SEP 2015
Accepted 5 MAR 2016
Accepted article online 12 MAR 2016
Published online 26 MAY 2016

Tracking multiple sediment cascades at the river network scale identifies controls and emerging patterns of sediment connectivity

Rafael J. P. Schmitt[1], Simone Bizzi[2], and Andrea Castelletti[1,3]

[1]Department of Electronics, Information, and Bioengineering, Politecnico di Milano, Piazza Leonardo da Vinci, Milano, Italy, [2]European Commission, Joint Research Centre, Institute for Environment and Sustainability, Water Resources Unit, Ispra (VA), Italy, [3]Institute of Environmental Engineering, ETH Zurich, Zurich, Switzerland

Abstract Sediment connectivity in fluvial networks results from the transfer of sediment between multiple sources and sinks. Connectivity scales differently between all sources and sinks as a function of distance, source grain size and sediment supply, network topology and topography, and hydrologic forcing. In this paper, we address the challenge of quantifying sediment connectivity and its controls at the network scale. We expand the concept of a single, catchment-scale sediment cascade toward representing sediment transport from each source as a suite of individual cascading processes. We implement this approach in the herein presented **CA**tchment **S**ediment **C**onnectivity **A**nd **DE**livery (CASCADE) modeling framework. In CASCADE, each sediment cascade establishes connectivity between a specific source and its multiple sinks. From a source perspective, the fate of sediment is controlled by its detachment and downstream transport capacity, resulting in a specific trajectory of transfer and deposition. From a sink perspective, the assemblage of incoming cascades defines provenance, sorting, and magnitude of sediment deliveries. At the network scale, this information reveals emerging patterns of connectivity and the location of bottlenecks, where disconnectivity occurs. In this paper, we apply CASCADE to quantitatively analyze the sediment connectivity of a major river system in SE Asia. The approach provides a screening model that can support analyses of large, poorly monitored river systems. We test the sensitivity of CASCADE to various parameters and identify the distribution of energy between the multiple, simultaneously active sediment cascades as key control behind network sediment connectivity. To conclude, CASCADE enables a quantitative, spatially explicit analysis of network sediment connectivity with potential applications in both river science and management.

1. Introduction

Connectivity in fluvial systems embodies magnitude and timing of transport processes ranging from the routing of discharge [*Rinaldo et al*., 2006], to the travel of aquatic species, pathogens [*Gatto et al*., 2013], or sediment [*Czuba and Foufoula-Georgiou*, 2014]. Sediment connectivity is a determinant of river geomorphic processes [*Hooke*, 2003] and concerns fluvial ecosystem integrity, access to water resources [*Trush et al*., 2000], delivery of nutrients or pollutants [*Walling*, 1983], natural hazard risks [*Bechtol and Laurian*, 2005], and, ultimately, human livelihoods in fluvial systems [*Habersack et al*., 2014].

Sediment connectivity in river networks describes the delivery from sediment sources to sinks in the domains of magnitude, transport time, and delivered grain size [*Bracken et al*., 2015]. The concept encapsulates multiple spatiotemporal scales with a potential nexus between reach-scale entrainment, transport, and deposition processes, network topology [*Bracken et al*., 2015], and network scale patterns of sediment redistribution [*Brierley et al*., 2006]. Numerical models could greatly advance the study of connectivity because of the multiple involved process domains and spatiotemporal scales, which limit empiric studies of connectivity typically to small, well studied catchments [e.g., *Fryirs et al*., 2007b].

Different numerical approaches to study network scale sediment transfers, channel adjustments, and connectivity have been introduced. Stream-power based approaches on the single river [*Bizzi and Lerner*, 2016] and network [*Parker et al*., 2015] scale predict deposition or erosion dominated reaches with high accuracy based on current hydro-morphologic forcing. Nevertheless, they do not consider sediment transfers as

additional driver for channel adjustment. *Benda and Dunne* [1997] used distributed sediment mass-balances to study how the spatial distribution and stochastic activation of sediment sources resulted in spatio-temporal patterns of flux along a sediment cascade. *Wilkinson et al*. [2006] applied a similar approach to identify depositional reaches at the network scale. Both approaches pointed out potential sediment sinks, but could not explicitly identify and quantify sediment source-sink relationships or sediment provenance. This limitation was due to the aggregation of sediment transport from all sources into a single bulk measure. *Czuba and Foufoula-Georgiou* [2014], in contrast, implemented common sediment transport formulas in a graph-theoretic framework. The approach allowed the movement of individual sediment parcels to be traced through a river network, identifying both temporal trajectories of sediment parcels and resulting network scale dynamics [*Czuba and Foufoula-Georgiou*, 2015]. Nevertheless, this dynamic connectivity approach did not explicitly quantify sediment source-sink relations, because sediment parcels were not subject to local transport capacity limitations and deposition.

All of the above studies provided insight into specific aspects of network sediment connectivity. Nevertheless, to date, no approach explicitly appraises multiple sediment source-sink transfers, which would be a requirement for integrated assessments of sediment connectivity [*Bracken et al*., 2015]. In this paper, we combine previous approaches into a novel network scale modeling approach to quantify sediment connectivity. The key novelty of the approach is that the transport of each sediment input is conceptualized as an individual cascading process. In the CASCADE (**CA**tchment **S**ediment **C**onnectivity **A**nd **DE**livery) modeling framework, each sediment source is assessed as the beginning of a new sediment cascade. In this way, CASCADE allows analyses of connectivity both from a source or a sink perspective. CASCADE quantifies how the sediment that is supplied from a source is delivered to all downstream sinks. From a sink perspective, CASCADE traces back all sediment inputs to their sources and determines the total local sediment flux, the flux of each grain size, the spatial distribution of sources, and the connection times between sources and sinks. From this information, statistical properties of connectivity can be derived. This process-related information opens up opportunities for reach- and network scale studies of sediment connectivity from both a research and a management perspective.

In this paper, we focus on the theoretical framing and the formulation of the CASCADE modeling framework. We show for the Da River basin in SE Asia (China, Vietnam, Laos; drainage area: 50,570 km^2) how the CASCADE modeling framework can be initially parameterized based on remote sensing data that are available for most river systems world-wide. We present the novel kind of connectivity information that results from CASCADE. We use CASCADE to demonstrate how cascade-specific rates of sediment entrainment, transport, and deposition scale into spatiotemporal connectivity patterns at both local and network scales. We analyze these patterns to clarify how different factors, above all the distribution of energy between different sediment cascades, and the spatial distribution and properties of sediment sources result in different patterns and statistical properties of network connectivity.

2. The CASCADE Approach

The CASCADE framework represents the sediment transport from all sediment sources through the river network as individual cascading transport processes. An individual transport rate is assigned to each cascading process as a function of local (i.e., specific to a river reach) hydro-dynamics, morphology, and transported grain size. Transport capacities are derived from these parameters through network scale implementation of standard sediment transport formulas. A graph-based routing scheme was implemented based on recent advances in describing landscape [e.g., *Cheung et al*., 2015; *Heckmann et al*., 2015] and fluvial [*Czuba and Foufoula-Georgiou*, 2014, 2015] sediment connectivity, resulting in a spatially explicit map of transport rates for each sediment cascade. The basic approach is clarified in Figure 1: the river network (Figure 1a) is transferred into a directed acyclic graph (river graph), which represents the network topology as a set of nodes and edges (Figure 1b). For example, for the network shown in Figure 1, the original set of five reaches is transferred into sets of five edges (see numbers in Figure 1b) and six nodes. Multiple sediment sources are active in the river network (Figure 1c, roman numbers). Each sediment source has a specific grain size (visualized by the dot size) and sediment supply. The sediment from each source is transported along an individual sediment cascade. Therefore, the river graph is expanded to represent attributes, e.g., grain size or sediment flux, of each cascade separately (Figure 1d). Each cascade is assigned a specific

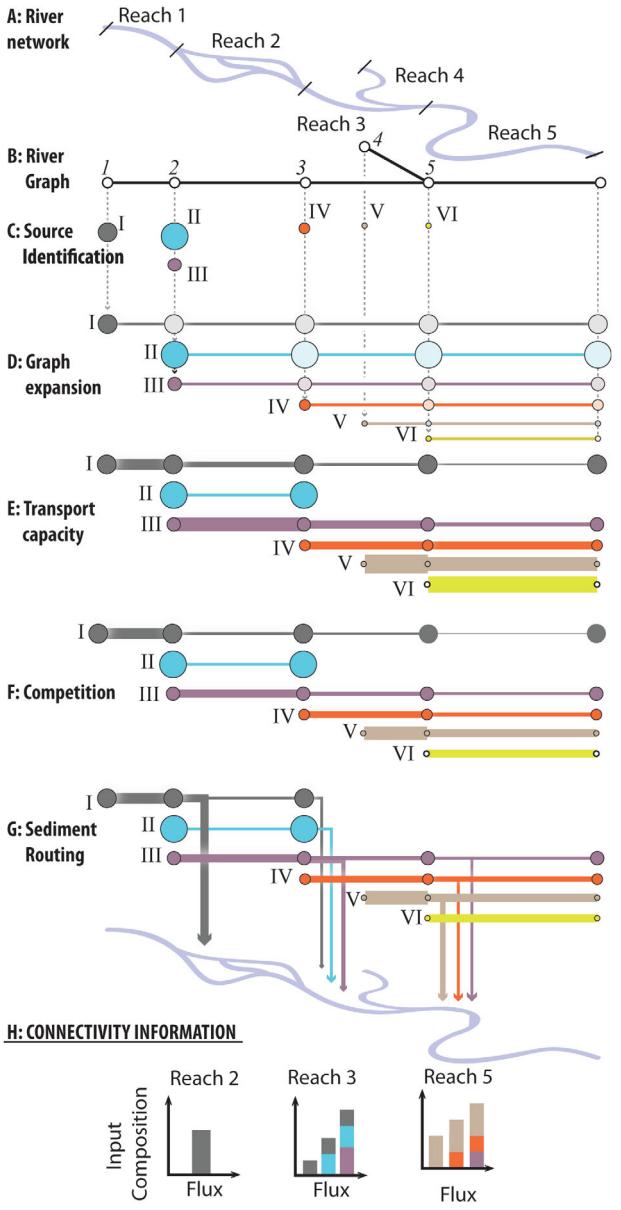

Figure 1. Key concepts and steps behind the CASCADE modeling framework. (a and b) Original river network and graph representation. (c) Identifying source locations and grain sizes. (d) Graph expansion. (e) Transport capacity scaling, line width indicates transport capacity. (f) Competition reduces the original transport capacity (compare linewidth in Figures 1e and 1f). (g) Cascade specific, edge-to-edge sediment routing discriminates cascade sediment fluxes. (h) Edges receive fluxes from multiple cascades, defining sediment flux, provenance, and sorting; and thereby connectivity of an edge.

transport capacity in each reach downstream of its source. Transport capacities are calculated using standard sediment transport formulas based on the grain size of the source and the local hydraulic forcing in the downstream reaches (Figure 1e, linewidth represents transport capacity). For example, in reach 5 (Figure 1e) cascade III has a lower transport capacity than cascade V, because cascade V transports a smaller grain size. Sediment cascades can be interrupted if their grain size cannot be entrained in a downstream reach (Figure 1e, cascade II in reach 3). The calculated transport capacity does not yet consider the presence of multiple sediment cascades in the same reach. The more cascades that are present in a river reach, the less energy is available for each cascade. This competition for the available energy (Figure 1f) reduces the transport capacity for each cascade (compare line-widths between Figures 1e and 1f). The functioning of each cascade is determined based on sediment supply and the local competition corrected transport capacity (Figure 1g). It should be noted that no new sediment is taken up along a sediment cascade downstream of its source. Otherwise, a single cascade would encompass multiple sets of source-sink relationships and no unique connectivity information could be derived. Sediment is deposited if the input into a reach exceeds the local transport capacity (Figure 1g, downward arrows). A sediment cascade is interrupted as soon as the entire input is deposited (Figure 1g, sediment cascade I is interrupted for that reason in reach 3). Sinks are defined as reaches where a cascade deposits sediment (Figure 1g, for cascade III there are two sinks: reach 3 and 5). As a consequence, a reach can act as a sink for multiple cascades (e.g., in Figure 1g, Reach 5 acts as sink for cascades III, IV, and V). The assemblage of cascades connected to a reach defines sediment provenance (i.e., the location of sources), connection time to each source, and the sorting and magnitude of the total sediment delivery to a reach (Figure 1h).

2.1. Graph Notation

This section introduces key concepts of the multi-cascade sediment routing and the related notation. The river network is represented as a directed acyclic graph (DAG) $G=\{N, E\}$. G comprises N indexed nodes and E is a spanning set of edges (each edge represents a river reach). The cardinality of E is e and the cardinality of N is n (e.g., in Figure 1b, e = 5 and n = 6). $n \in N$ is a node in N, $e \in E$ is an edge in E.

A set A_e of attributes is associated to each edge representing the properties of the associated river reach. The set A_e can be split in four subsets $A_e(1)\cdots A_e(4)$ of cardinality $a_e(1)\cdots a_e(4)$, each representing a different domain. The first domain is the local geomorphic state [*Czuba and Foufoula-Georgiou*, 2014], which is defined by width, gradient, length, and drainage area of a reach (W_{AC_e}, I_e, L_e, A_{D_e}). The second domain is the hydraulic state, a probability distribution function of water flow stage and flow velocity ($f(h_e)$, $f(v_e)$). The third domain describes the grain sizes delivered from upstream sources. The fourth domain defines the sediment transport state in a reach. This includes, e.g., Q_{S_e} (sediment transport capacity), Θ_e (sediment flux), t_{Se} (sediment residence time), and any other measure of local sediment transport. The transport state is derived from the geomorphic, hydraulic, and grain size states using empiric sediment transport formulations.

Let now Γ be the full set of sediment cascades. The cardinality g of Γ is equal to the number of all active sediment sources S in the river network. If $\varsigma \in S$ is a specific sediment source, then γ_ς is the associated sediment cascade that transports grain size d_ς. Next, the sediment pathways are defined. A pathway $\kappa \subseteq E$ is the set of edges along which a sediment source ς is topologically connected to the terminal node at the basin outlet (Ω). Finding all cascades that pass through an edge e defines $\Gamma_e \in \Gamma$: the set of cascades that are connected to edge *e*. Then, $S_e \in S$ are all sources connected to *e*. The cardinality g_e of Γ_e equals the cardinality s_e of the set S_e. For example, in Figure 1d, $\Gamma_3 = \{I, II, III, IV\}$ is the set of cascades originating from the sources $S_e = \{I, II, III, IV\}$ and passing through edge 3 ($g_3 = 4$).

The concept of multiple cascades that transport different grain sizes d_ς, and that therefore operate at different rates, requires expanding the sediment transport state in each edge. In Figure 1d, for example, there are three sediment cascades in edge 2 ($\Gamma_2 = I, II, III$). Each cascade has a different transport capacity (Figure 1e,f) and sediment flux (Figure 1g) in edge 2 as a function of the source grain size. Therefore, the cardinality of $A_e(4)$ is expanded into $a_e(4)' = a_e(4) \cdot g_e$ and, correspondingly, also the full cardinality of A_e is expanded into a_e'. Hence, the attribute set A_e is expanded to include the original attribute subsets $A_e(1), A_e(2), A_e(3)$ and the multiple set of $A_e(4)'$. Hence, for edge 2 in Figure 1, $g_2 = 3$ and $a_2(4)' = 3$.

3. Formulation of the CASCADE Modeling Framework

This section explicitly describes the formulation of the CASCADE modeling framework at the network scale. The model requires a fully parameterized fluvial graph as input. The parameterization of the graph is case-study dependent and therefore is introduced later for a real case study. This section focuses instead on the implemented generic framework for sediment routing.

3.1. Transport Capacity Scaling

Sediment is mobilized in a reach and transported downstream if the local flow energy exceeds the threshold for sediment entrainment. The magnitude and frequency of flow events determines, therefore, how much sediment of a given grain size can be transported over a given time-span (e.g., over a year) in a reach. Processes involved in the transport of different grain size classes differ significantly. For example, fine silt and clay are mostly transported in suspension (wash load, suspended load), gravel and cobble fractions are transported on the river bed (bed-load), while sand fractions can be transported either in suspension or on the bed, depending on the hydraulic conditions. Empirical formulations that relate sediment transport rates to local hydraulic conditions are therefore applicable to a specific grain size range, only. Therefore, CASCADE uses two different sediment transport formulas to scale the sediment multigraph into a representation of local transport capacity [*Czuba and Foufoula-Georgiou*, 2014], one for sand [*Engelund and Hansen*, 1967], and one for gravel [*Wong and Parker*, 2006]. The dimensionless transport capacity q_{S*e}^{ς} for grain size d_ς in edge *e* is defined as:

$$q_{S*e}^{\varsigma} = \begin{cases} \dfrac{0.05}{C_{fe}^{\varsigma}} \cdot \tau_{*e}^{\varsigma 5/2}, \text{ if } d_\varsigma < 2\times10^{-3}\, m \\ \alpha \cdot \left(\tau_{*e}^{\varsigma} - \tau_{*c_e}\right)^{\beta}, \text{ else} \end{cases} \tag{1}$$

In these equations, α and β are the only constants and directly derived from *Wong and Parker* [2006] ($\alpha = 3.97$, $\beta = 1.5$). C_{fe}^{ς} is the local friction factor,

$$C_{f_e}{}^{\varsigma} = \frac{2 \cdot g \cdot I_e \cdot h_e}{v_e{}^2}, \tag{2}$$

the dimensionless shear stress $\tau_{*_e}^{\varsigma}$ is derived from

$$\tau_{*_e}{}^{\varsigma} = \frac{I_e \cdot h_e}{R \cdot d_{\varsigma}}, \tag{3}$$

where R is the relative density of sediment. The dimensionless transport capacity is transferred into a dimensionful value through

$$q_{S*_e}^{\varsigma} = \frac{q_{S_e}^{\varsigma}}{\sqrt{R \cdot g \cdot d_{\varsigma}{}^3}}. \tag{4}$$

The final result from solving equation (4) is the volumetric sediment transport $q_{S_e}^{\varsigma}$ $[m^2 d^{-1}]$ for d_{ς} in e per unit channel width.

$q_{Se}{}^{\varsigma}$ is an instantaneous value under given hydraulic conditions. Deriving the actual transport capacity of an edge requires information on the magnitude and frequency of flows. Therefore, CASCADE requires a hydrograph $\boldsymbol{Q_e}$, a vector of n_{tot_e} flow observations for each edge. $\boldsymbol{Q_e}$ is divided into p percentiles and the mean discharge value $Q_e(p)$ in each of the p percentiles is derived. We define the percentiles as $-4\sigma \ldots +4\sigma$ of a standard normal distribution $(0.1\%, 2.3\%, 15.9\%, 50\%, 84.1\%, 97.7\%, 99.9\%)$.

CASCADE includes a hydrodynamic solver (Appendix A). The solver calculates mean flow velocity and flow stage, $v_e(p)$ and $h_e(p)$, for each $Q_e(p)$ (hence p sets of $v_e(p)$, $h_e(p)$ for each edge). CASCADES calculates the mean transport capacity for d_{ς} in each discharge percentile $(q_{Se}{}^{\varsigma}(p))$ by inserting d_{ς}, $v_e(p)$, and $h_e(p)$ into equations (1–4). The total transport capacity for d_{ς} in the p – th percentile follows from $q_{Se}{}^{\varsigma}(p)$ and the number of observations within the p – th percentile, $n_{p_e}(p)$

$$q_{S,tot_e}^{\varsigma}(p) = q_{S_e}{}^{\varsigma}(p) \cdot n_{p_e}(p). \tag{5}$$

The mean annual transport capacity for d_{ς} (and therefore for cascade γ_s) in edge e is

$$q_{S,annual_e}^{\varsigma} = \frac{\sum_{k=1}^{p} q_{S,tot_e}{}^{\varsigma}(k)}{n_{tot_e}} \cdot 365. \tag{6}$$

where n_{tot_e} is the total number of observations available for edge e. $q_{S,annual_e}^{\varsigma}$ is converted from (m^2 yr^{-1}) to mass (kg yr^{-1}) by

$$Q_{S_e}^{\varsigma} = q_{S,annual_e}^{\varsigma} \cdot W_{AC_e} \cdot \rho_S, \tag{7}$$

where $\rho_S = 2600$ kg m^{-3} is the sediment density.

In theory, CASCADE can calculate a specific sediment transport capacity for each of the n_{tot_e} discharge observations in all edges. Nevertheless, the computational demand of this approach is substantial, even for small river systems. Calculating $Q_{S_e}^{\varsigma}$ in a river system with 100 edges, in which each edge contains an average of $g_e = 10$ different cascades and 10 years of daily discharge observations are available ($n_{tot} = 3650$) would require calculation of 3.65E6 pairs of v_e and h_e, and then $Q_{S_e}^{\varsigma}$. Using the discharge percentiles instead of the full hydrographs reduces the computational demand significantly (i.e., by replacing n_{tot} by n_p only p^* 1E3 pairs of v_e and h_e need to be calculated if p percentiles are used). Dissecting the hydrographs using the σ-intervals rather than constant intervals considers the potential impact of rare, but high magnitude events on sediment transport [e.g., *Wolman and Miller*, 1960]

3.2. Competition

The sediment transport formulas that are implemented in CASCADE (equations (1–4), and equations (5–7)) derive the transport capacity for a single grain size, only. They do not consider that the transport capacity for d_{ς} in edge e will be changed if multiple grain sizes are present that compete for the locally available energy [e.g., *Wu et al*., 2003; *Hsu and Holly*, 1992; *Sutherland*, 1987]. Hence, $Q_{S_e}^{\varsigma}$ only represents the transport capacity for d_{ς} in e if there is only a single source connected to e. A competition factor is introduced to derive a competition corrected transport capacity ($Q_{S_e}^{\varsigma\prime}$) that considers the redistribution of energy between cascades. Empirical formulations that describe the simultaneous movement of multiple sediment fractions

[e.g., *Wilcock and Crowe*, 2003; *Wilcock*, 1998] could be included in CASCADE in future. For this study we used some high level formulations of the competition factor, instead. This approach is novel and allowed to study the impact of some high-level assumptions regarding the simultaneous transport of multiple grain sizes on network sediment connectivity.

We developed three different scenarios for competition. For all three scenarios we derive $Q_{S_e^\varsigma}'$ by multiplying $Q_{S_e^\varsigma}$ with an edge and source specific competition factor, F_e^ς, which we obtained from a dynamic competition function. The three scenarios vary in the calculation of both, $Q_{S_e^\varsigma}$ and F_e^ς. For scenario 1 and 2, a characteristic transport capacity is assigned to each edge *a-priori*. The characteristic transport capacity is defined as transport capacity for the local median grain size $Q_{S_e}(d_{50_e})$. d_{50_e} is estimated as median grain size of all upstream sources. $Q_{S_e}(d_{50_e})$ is calculated from equations (1)–(4) and equations (5)–(7) in all edges. $Q_{S_e}(d_{50_e})$ is then divided between the g_e sediment cascades.

For scenarios 1 and 2 holds:

$$Q_{S_e^\varsigma}'=F_e^\varsigma \cdot Q_{S_e}(d_{50_e}). \tag{8}$$

Scenario 1 postulates that sediment cascades with locally high transport capacity compete more effectively for transport capacity (local selective transport). Competition between sediment cascades is expressed as

$$F_e^\varsigma=\frac{Q_{S_e^\varsigma}}{\sum_{k\in\Gamma_e} Q_{S_e}^k} \tag{9}$$

according to *Wu et al*. [2003] and *Molinas and Wu* [2000]. The competition factor in this base-case compares the transport capacity of an individual cascade with the summed transport capacities for all other sediment cascades in edge *e*. Cascades with a locally higher transport capacity are assigned a higher share of $Q_{S_e}(d_{50_e})$. This implies that $Q_{S_e^\varsigma}'$ depends on local hydro-morphologic conditions and on the local grain size distribution. Finer grain sizes are transported preferentially, in this case [*Sutherland*, 1987].

Scenario 2 postulates that cascades with high initial sediment supply (Q_{S,in_ς}) rather than high local transport capacity compete more effectively for a share of $Q_{S_e}(d_{50_e})$. Thus,

$$F_e=\frac{Q_{S,in_\varsigma}}{\sum_{k\in\Gamma_e} Q_{S,in_k}}. \tag{10}$$

This follows the notion that the redistribution of transport capacity is strongly driven by sediment supply [*Hsu and Holly*, 1992]. Sediment fractions with higher supply, instead of finer grain sizes are transported preferentially.

Scenario 3 postulates, instead, that the local transport capacity of a cascade is a direct function of sediment supply.

$$Q_{S_e^\varsigma}'=F_e^\varsigma \cdot Q_{S,in_\varsigma}, \tag{11}$$

while F_e^ς depends on the local grain size distribution as in scenario 1 (equation (9)). This scenario follows the notion that the local bed-load transport capacity of an edge presents an adaptation to the presence of various grain size fractions on the bed-surface and sediment supply [*Parker*, 1990; *Dietrich et al*., 1989]. If cascades with the same supply are present in edge *e*, cascades with finer grain size will be more competitive. Without competition ($F_e^\varsigma=1$ for all cascades in all edges) all sediment cascades can pass through the river network without deposition, except if a grain size fraction cannot be entrained in an edge (i.e., $Q_{S_e^\varsigma}=0$ in equation (9)).

3.3. A Routing Scheme for Multiple Sediment Fractions

CASCADE implements a node-to-node sediment mass-balance to describe the functioning of the sediment cascades and the resulting sediment flux Θ between all pairs of sources and downstream edges. The sediment routing along a cascade is performed sequentially path-by-path. Hence, the sediment input into a cascade is routed along the entire cascade, (i.e., until the basin outlet or until the cascade is interrupted) before the routing of the next cascade begins. The calculation order can be defined as upstream-downstream (sediment cascades from more upstream sources are routed first), downstream-upstream (sediment cascades from more downstream sources are routed first), or random. The sediment flux in a cascade remains constant after the routing of the cascade is finished. Hence, we assume that sediment sources supply

sediment continuously at the same rate. CASCADE recalculates the competition factors in all edges after the routing of a sediment cascade is completed. The sediment flux along a cascade γ_ς in edge e is derived from a local mass balance

$$\Theta_e{}^{\varsigma}=\begin{cases}\Theta_{in_e}^{\varsigma}, \text{ if } \Theta_{in_e}^{\varsigma} < Q_{S_e}^{\varsigma\prime} \text{ (condition 1)}\\ Q_{S_e}{}^{\varsigma\prime}, \text{else (condition 2)}.\end{cases} \tag{12}$$

Hence, all sediment is routed downstream if the flux from the next upstream edge ($\Theta_{in_e}^{\varsigma}$) is smaller than the competition corrected transport capacity $Q_{S_e}^{\varsigma\prime}$ in edge e (condition 1). If $\Theta_{in_e}^{\varsigma}$ exceeds $Q_{S_e}^{\varsigma\prime}$, then only $Q_{S_e}^{\varsigma\prime}$ is routed downstream and the sediment cascade experiences deposition in edge e (condition 2). Sediment cascades can be disconnected ($\Theta_e{}^{\varsigma}=0$) based on two mechanisms: (a) because the local transport capacity is not sufficient to entrain d_ς in edge e, (b) because all or most of the sediment supply (i.e, a certain percentage of Q_{S,in_ς}) was deposited between the source ς and e. In here, we assume that a sediment cascade is interrupted after 95 % of Q_{S,in_ς} was deposited. Hence,

$$\Theta_e{}^{\varsigma}=0, \text{ if } \begin{cases}Q_{Se}{}^{\varsigma\prime}=0 \text{ (a)}\\ \Theta_e{}^{\varsigma} < 0.05\cdot Q_{S,in_\varsigma} \text{ (b)}.\end{cases} \tag{13}$$

$\Theta_e{}^{\varsigma}$ also defines the residence time of γ_ς in e

$$t_e{}^{\varsigma}=\frac{L_e}{v_{S_e}^{\varsigma}}, \tag{14}$$

where $v_{S_e}^{\varsigma}$ is the sediment travel velocity of d_ς in edge e, and L_e is the length of that edge. $v_{S_e}^{\varsigma}$ is defined as flux per cross-sectional area $A_{x_e}^{\varsigma}$ in which d_ς is transported. $A_{x_e}^{\varsigma}$ is a function of active channel width, W_{AC_e}, and the part of the water column, $\theta_e{}^{\varsigma}$, in which d_ς is transport. $\theta_e{}^{\varsigma}$ is calculated as $2.1\cdot d_\varsigma$ [*Church et al.*, 2012]. $v_{Se}{}^{\varsigma}$ becomes

$$v_{S_e}^{\varsigma}=\frac{\Theta_e{}^{\varsigma}}{A_{x_e}^{\varsigma}}=\frac{\Theta_e{}^{\varsigma}}{\theta_e{}^{\varsigma}\cdot W_{AC_e}}. \tag{15}$$

The sediment residence times for cascade γ_ς can be used to calculate the connection time along any set of connected edges that participate in $\kappa_\varsigma^{\Omega}$. E.g., let ε be a set of connected edges along the pathway $\kappa_\varsigma^{\Omega}$. The total connection time for γ_ς along the ε ($T_\varepsilon^{\varsigma}$) is then

$$T_\varepsilon^{\varsigma}=\sum_{k\in\varepsilon} t_k{}^{\varsigma}. \tag{16}$$

From equations (14)–(16) it is evident that connection times in CASCADE are a direct function of sediment fluxes, sediment supply, competition, and the hydromorphological drivers in the river network along the edges ε. Fluxes and connection times are cascade specific. Hence, connectivity scales differently along the edges ε, if ε participates in multiple cascades.

Last, the total flux of sediment in an edge, Γ_e, is defined as the sum of sediment flux along all cascades Γ_e in that edge:

$$\Theta_e=\sum_{k\in\Gamma_e}\Theta_e{}^{k}. \tag{17}$$

4. Implementing CASCADE at the River Network Scale

This section introduces a possible approach for parameterizing CASCADE for a large river network in SE Asia. This section first introduces the case study and describes (1) the derivation of fluvial graph and geomorphic states, (2) estimation of edge hydrographs, and (3) parameterization of sediment sources and grain sizes. CASCADE was implemented for the Da River system which is shared between Vietnam, China, and Laos (100° 22′ 30.587″ E, 24° 51′ 10.576″ N, and 105° 25′ 13.241″ E, 20° 35′ 44.263″ N) (Figure 2). The basin of the Da River covers an area of 50,570 km^2 and an elevation range from 3143 to 18 m asl. The Da River basin provides the major sediment input into the Red River Basin [*Le et al.*, 2007], which ranks 9th in the world in terms of sediment output [*Milliman and Meade*, 1983].

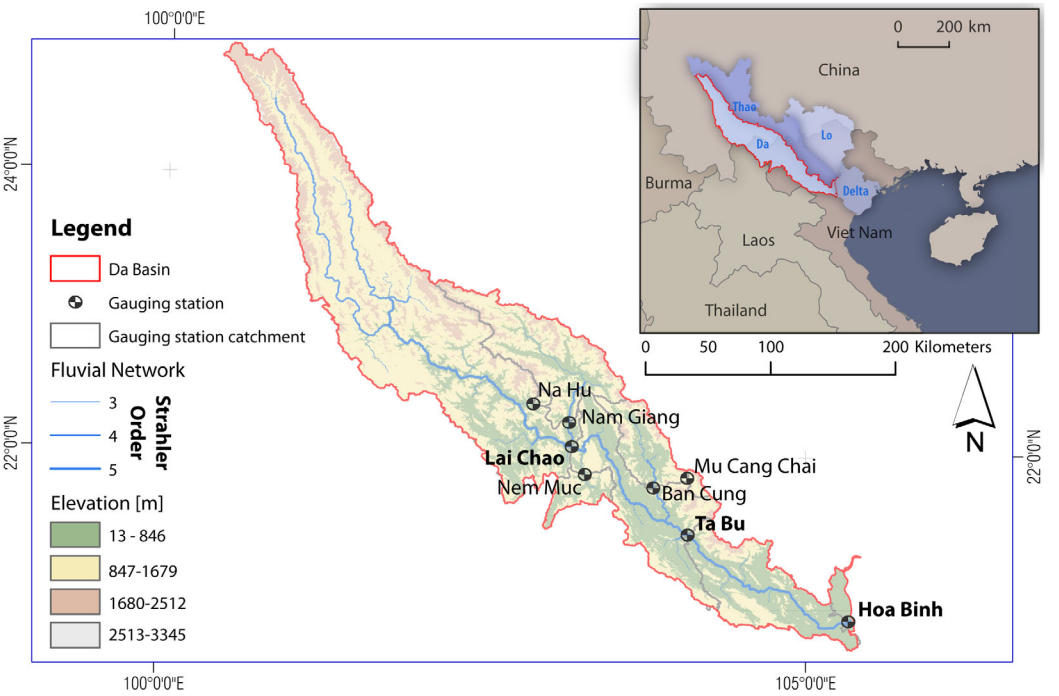

Figure 2. Overview over the Da River Basin and the available gauging stations. Bold names indicate gauging stations for which total suspended sediment measurements are available. The small map indicates the location of the Da-River Basin within the Red River drainage system.

4.1. Deriving a Fluvial Multigraph

4.1.1. Delineating the River Network and Measuring Reach Geomorphic States

We derived the river network from a DEM with 30 m resolution (ASTER GDEM) using the standard procedure of DEM filling and flow routing outlined in *Tarboton et al.* [1991]. The river network was extracted using a drainage area threshold of 125 km^2. The resulting river network has a total length of 7433 km length with Strahler Orders ranging from 1 to 5. There are 5 major lateral tributary systems (with $A_D > 2500$ km^2). The network was first dissected at all confluences. All resulting reaches were split after a maximum of 5000 m, hence all reaches had a length 5000 m or shorter. This resulted in a total of 2123 reaches of which 949 had the full length of 5000 m (mean length 3511 m). CASCADE transferred the river network into a graph representation of 2123 edges and 2124 nodes. The geomorphic state was determined for all edges. Gradients were calculated from the length of an edge and the elevation difference between the start and end node. The drainage area was measured at the start and end nodes of an edge and the mean of both values was assigned to the edge. CASCADE calculated the active channel width, W_{AC}, using an empiric scaling law that was derived for the basin under study in a previous study

$$W_{AC} = A_D^{m_{AD-W}} * I^{n_{AD-W}} \tag{18}$$

with ($m_{AD-W} = 0.476$, $n_{AD-W} = -0.07675$) [*Schmitt et al.*, 2014].

4.1.2. Deriving Reach Hydraulics

This step concerns deriving reach-level hydrographs, dissecting each hydrograph into p flow percentiles, and calculating hydraulic conditions in each flow percentile. The local hydrograph was derived by down-

Table 1. Overview Over the Available Hydrologic Observations

Station Name	Ban Cung	Hoa Binh	Lai Chau	Mu Cang Chai	Na Hu	Nam Giang	Nam Muc	Ta Bu
Period	1962–2011	1956–2011	1957–2011	1980–2008	1968–2011	1965–2011	1960–2011	1961–2011
Ad (km^2)	2577	50570	27151	270	147	5783	3119	44603
Mean Q (m^3 s^{-1})	172.11	1692.34	1138.52	5.77	13.59	272.93	85.05	1517.79
Mean Q (mm d^{-1})	5.77	2.89	3.62	1.85	7.99	4.08	2.36	2.94

scaling observed hydrographs with a scaling-law based on A_D. Eight long term discharge records (mean record length 47 yrs, daily resolution) were available. Gauging stations covered a range from very small upland (A_D=147 km^2) to major lowland rivers (A_D=50,570 km^2). For location and details of all available discharge records refer to Figure 2 and Table 1. The catchment of each flow gauging stations marks one of eight subbasins. For the down-scaling we applied an edge-specific scaling factor J_e,

$$\boldsymbol{Q_e} = J_e \cdot \boldsymbol{Q_{SB}}, \tag{19}$$

where $\boldsymbol{Q_e}$ is the hydrograph assigned to edge e, and $\boldsymbol{Q_{SB}}$ is the observed hydrograph at the next downstream gauging station. We calculated J_e from

$$J_e = \frac{Q_{1.5_e}}{Q_{1.5_{SB}}}, \tag{20}$$

where $Q_{1.5_e}$ is the 1.5 year discharge in edge e and $Q_{1.5_{SB}}$ is the 1.5 year discharge in the next downstream gauging station. $Q_{1.5_e}$ was estimated using a scaling law derived from the same 8 gauging stations, which reached a high R^2 (0.94) [*Schmitt et al.*, 2014]. Hence, J_e can be transformed into

$$J_e = \frac{a * A_D^b}{Q_{1.5_{SB}}} \tag{21}$$

with a=1.321 and b=0.82. $\boldsymbol{Q_e}$ is therefore a nonlinearly down-scaled version of an observed hydrograph. CASCADE split the reach hydrographs for each of the 2123 edges into $p = 8$ percentile values. Then, CASCADE calculated the mean discharge in each percentile and the 1.5 year discharge for each of the 2123 edges. CASCADE used the hydraulic solver (see Appendix A) to calculate $v_e(p)$ and $h_e(p)$ for all $Q_e(p)$, as well as $v_e(Q_{1.5})$ and $h_e(Q_{1.5})$.

4.1.3. Network Scale Characterization of Sediment Sources

Identifying sediment sources and the supplied grain size is a key step for building the CASCADE modeling framework. Such information is not available for the river network under study, neither will it be for most river networks. Therefore, grain sizes in CASCADE can be initialized on the network scale using an analytic approach. This approach assumes that each edge is the source of one single grain size d_ς, and that d_ς is a direct function of bankfull hydraulics, $v_e(Q_{1.5})$ and $h_e(Q_{1.5})$. This procedure is based on the assumptions that (a) the maximum bed shear stress occurs under bankfull hydraulic conditions and, (b) that the 1.5 year discharge is a good approximation of the bankfull discharge [*Knighton*, 1984]. The maximum shear stress defines the equilibrium grain size that can persist in edge e, while smaller grain sizes are entrained [*Andrews*, 1983]. We then assumed that the grain size of sediment produced in e is proportional to the equilibrium grain size. This results in $S = 1 \cdots 2123$ sediment sources that deliver sediment along $\Gamma = 1 \cdots 2123$ sediment cascades. The detailed calculation procedure for deriving d_ς is presented in Appendix B.

Estimating grain sizes and locating sediment sources at the network scale is a major challenge in setting up CASCADE. The application of a single grain size throughout the basin has been successfully applied to model sediment transport in smaller catchments [*Czuba and Foufoula-Georgiou*, 2015, 2014; *Wilkinson et al.*, 2006]. Nevertheless, we assumed that using a single grain size can hardly result in relevant results given the wide range of hydromorphologic conditions in the river network under study. For example, assigning a single sandy grain size to all reaches would result in a major overestimation of sediment outputs from steep upstream reaches and an underestimation of sediment transport in higher-order, downstream reaches. We tackle this problem by transforming the available hydrologic and topographic information into a consistent estimate of grain sizes. The resulting spatial distribution, probability distributions, and correlations between grain-size d_ς and hydraulic parameters h_e, v_e, and $\tau_{*c_e^\varsigma}$ in the basin under study are reasonable and we discuss and present results in detail in Appendix C. All sources are characterized by a specific supply Q_{S,in_ς}. Herein, we initialized sediment sources with

$$Q_{S,in_\varsigma} = Q_{S_e}^{\varsigma'}. \tag{22}$$

Hence, the sediment supply of d_ς is equal to the competition corrected transport capacity for d_ς in the edge where ς is located. This implies that sediment sources are only detachment but not supply limited. Nevertheless, the rate of detachment will be strongly reduced for sources that are located in an edge with many

active cascades and strong competition. Finally, CASCADE applies a shortest path algorithm [*Dijkstra*, 1959] to determine the pathway $\kappa_{\varsigma}^{\Omega}$ for all sources.

4.2. Sediment Routing and Competition

CASCADES loops trough all $\varsigma \in S$ and calculates the transport capacity for all edges $e \in \kappa_{\varsigma}^{\Omega}$ using equations (1)–(7). At this stage, the sediment pathway for d_{ς} can be interrupted if d_{ς} cannot be entrained in a downstream edge (equation (13a)). After this step, each edge was traversed by an average of 26.7 sediment cascades. Competition between these cascades for the locally available energy was considered through the dynamic competition factor. We performed three separate runs of CASCADE, considering a different competition scenario in each run.

4.3. Scenario and Sensitivity Analysis

The main aim of this paper is to introduce the CASCADE modeling framework and to provide evidence for how the derived information can provide novel insights into network sediment connectivity. We also test the sensitivity of cascade to some key assumptions. A full analysis of the distributed, network scale sensitivity of CASCADE is beyond the scope of this article.

Therefore, we focus on the impact of competition scenarios, because competition interlinks empirical sediment transport calculations to more conceptual aspects of sediment connectivity and of the CASCADE modeling framework. There is no empirical information on sediment connectivity available for validating results in the network under study. Accordingly, we resort to a comparative analysis of the three scenarios, and match them to empirical observations and generic concepts of network scale sediment connectivity. In a similar comparative approach, we evaluate the impact of grain size initialization on network connectivity. CASCADE in its current implementation considers only bed-load (i.e., sand or coarser fractions), while for the basin under study only observations of total suspended solids (TSS) are available [*Vinh et al*., 2014; *Le et al*., 2007]. Therefore, we calculate the ratio between observed TSS and modeled bed-load, and compare results to available, global and regional observations [*Turowski et al*., 2010; *Bravard et al*., 2014]. Additionally, a single estimate of median grain size in the main stem of the Da River was available from *Vinh et al*. [2014].

5. Results

Here, we present the outcomes of the CASCADE modeling framework for the Da River system. The analyses clarify how CASCADE allows assessments of all domains of connectivity at the reach scale, as well as at larger (multireach or network) scales. Results on both scales are analyzed with a focus on the impact of competition upon sediment connectivity. The execution of the CASCADE model for the Da River system is also shown in Movie S1.

5.1. Reach-Scale Connectivity

The reach scale analysis focuses on a single reach on the main stem of the Da River (Figure 3). The reach is located at the confluence of a major sandy tributary with the main stream, see also Figure 8 (tributary 3), and identical with Lai Chau (LC) gauging station (Figure 2). We calculate the connection times between all connected sediment sources and the reach under study. Connection times are used to group incoming sediment cascades into bins. The bins are defined between the 5–95 percentile of connection times in steps of 5%. The 5% (p_5), 50% (p_{50}), and 95% (p_{95}) percentiles are analyzed in more detail. The cumulative number of established connections increases with each percentile and p_{100} represents full connectivity. Hence, all upstream sources that can connect to the reach under study are connected. We identify which cascades connect to the reach under study within which bin of connection time, where their respective sources are located, and which fraction of the total input within that bin they provide. The analysis focuses on scenario 1 and 3, the end members between a local and a supply controlled perspective on sediment competition (for results of scenario 2 see Appendix D).

Scenario 1 results in a heterogeneous spatial pattern of sources for small connection times (p_5, p_{50} in Figure 3a). The reach under study connects equally to the main stem and to the major tributary within p_5. Preferential connectivity occurs to some reaches in lateral, mountainous drainage systems for p_5. These reaches present isolated sediment sources with a small grain size which connect efficiently to the downstream network. Hence, the grain sizes delivered within p_5 from these remote sources are relatively fine. The median

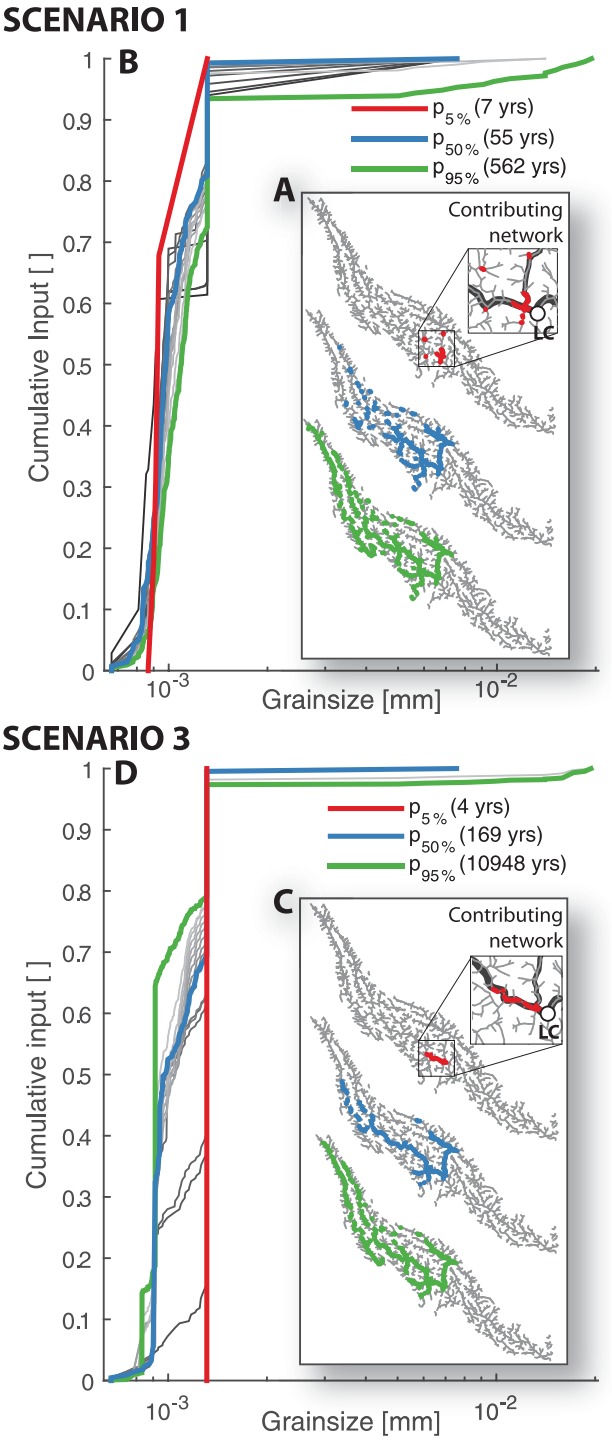

Figure 3. Reach connectivity for scenario 1 (a, b) and 3 (c, d) in terms of sediment delivery and source areas for different percentiles of connection time. The reach under study is identical with Lai Chau (LC) gauging station. Cutouts in Figures 3a and 3c clarify the spatial distribution of sources for very short (5% percentile) connection times.

delivered grain size increases with increasing connection time when cascades which transport large grain sizes also connect to the reach under study (Figure 3b).

For scenario 3, the reach under study connects only to reaches along the main stem for small connection times (Figure 3c, p_5). Reaches in the major lateral tributary and more upstream in the main stem connect within p_{50}. Smaller lateral tributaries are connected only above p_{50}. Preferential connectivity is limited to few reaches. The grain size delivered within p_5 is homogeneous, reflecting the grain size of sources located in the main stem. Delivered grain sizes fine for longer connection times as more upstream reaches connect to the reach under study (Figure 3d). The median grain size of delivered sediment under full connectivity (p_{95}) differs between the two scenarios even though nearly the same upstream sources are connected. This is because fluxes from each source are different between scenarios, which impacts upon the sediment composition in the reach under study.

5.2. Basin Scale Sediment Redistribution

The previous analysis indicated a significant impact of competition on reach connectivity. In this section, we enlarge the analysis and study the deposition trajectories from all sources located along the main stem of the Da River. Each trajectory is defined by the sediment conveyance ratio along a sediment cascade. The sediment conveyance ratio describes which percentage of the sediment supply from source ς is delivered to a downstream edge e. Hence, the inverse of the sediment conveyance ratio describes which percentage of the sediment supply from ς is deposited along the pathway κ_{ς}^{e} (Figures 4a and 4b). We also analyze the sediment conveyance ratio on the network scale between all ς and the basin outlet node Ω. This analysis identifies preferential connections on the network-scale and the sediment recruitment areas in which sediment sources are located that deliver sediment to the basin outlet. (Figures 4b and 4d).

Scenario 1 results in an unstructured pattern of deposition along the main stem. Longitudinal organization, e.g., due to tributaries, is absent (Figure 4a). There is no upstream-downstream gradient in the sediment

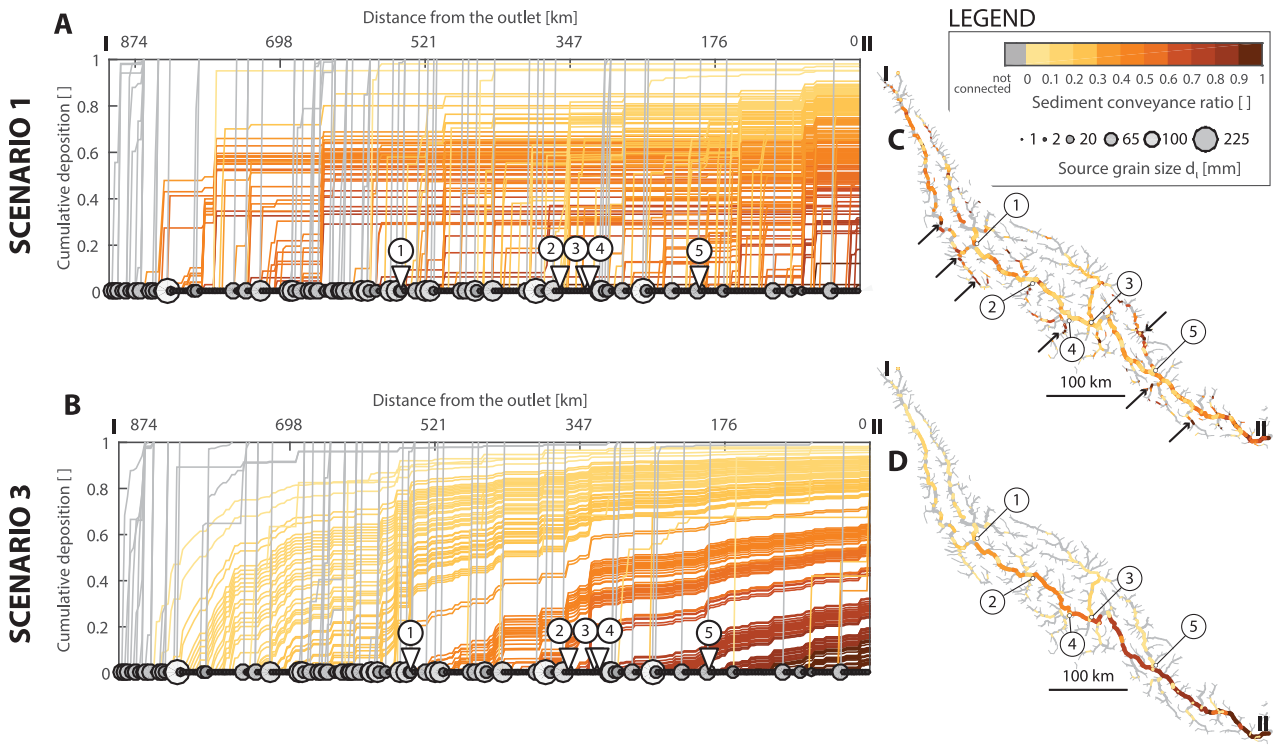

Figure 4. Network connectivity for scenario 1 (a, c) and 3 (b, d). Figures 4a and 4b show deposition trajectories (y-axis), respectively the sediment conveyance ratio (line color), along the main stem of the Da River. Dots indicate the source grain size d_s of each cascade (identical between scenarios). Numbers and triangles indicate the location of major tributaries ($A_D > 2500 km^2$, see also Figure 8). The sediment conveyance ratio is also mapped on the network scale throughout the river basin (Figures 4c and 4d). Arrows in Figure 4c indicate some hotspots of sediment recruitment.

conveyance ratio, i.e., no correlation between the distance of a source to the outlet and its connectivity to the outlet. Scenario 3 results, instead, in a continuous deposition and a clear upstream-downstream gradient in the sediment conveyance ratio along the river. Sediment delivery is longitudinally structured by tributaries into distinct bands (Figure 4b). Deposition is emphasized for cascades that begin close to a confluence and that still have a high sediment conveyance ratio at the confluence. Cascades from sources between confluences 1 and 2 are, for example, subject to much stronger deposition at confluence 2 then cascades from sources upstream of confluence 1. This is because the latter already deposited the majority of initial sediment inputs further upstream. Hence, a higher sediment flux increases the sensitivity to competition, e.g., at tributaries, under scenario 3. At the network scale, scenario 1 results in spatially discrete hot-spots of recruitment (Figure 4c, see arrows). Sediment cascades from these hot-spots compete effectively and reach the basin outlet without major deposition (conveyance ratio close to 1). For scenario 3, hotspots of recruitment are nearly absent (Figure 4d). There is a clear upstream - downstream gradient in sediment conveyance ratio. This gradient is a function of network hierarchy, with tributaries delivering less sediment to the basin outlet than the main stem. Results for scenario 2 are reported in Appendix D.

5.3. Patterns of Sediment Disconnectivity

Finally, we analyzed where disconnectivity occurs. Disconnectivity refers to sediment cascades that are disconnected from the basin outlet, either because the most of the sediment supply from its source is deposited, or because the supplied grain size cannot be entrained in a downstream reach. The analysis of disconnectivity includes (a) identifying the spatial distribution of sources that do not connect to the basin outlet and, (b) locating edges where the respective sediment cascades are interrupted. These edges can be considered potential in-channel sediment stores which could convert into sources. Though not considered in this paper, the frequency of such an activation would link to hydro-climatic conditions that result in extreme flow events, and the local morphologic conditions that would define a maximum value for in-channel sediment accommodation. First we identify disconnected sources using sediment trajectories and

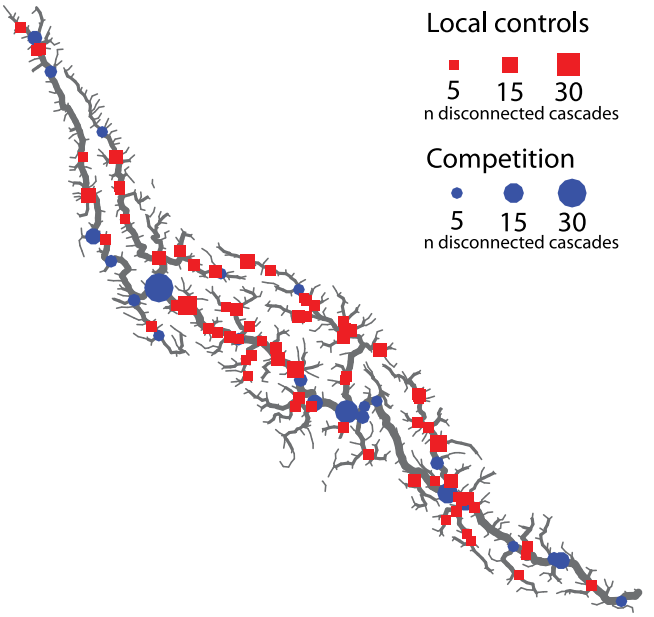

Figure 5. Hotspots of disconnectivity for scenario 3. Red squares and blue dots indicate edges where multiple cascades are interrupted either due to local hydro-morphologic controls or competition. The marker size indicates the number of interrupted cascades.

network scale patterns of sediment redistribution (i.e, all gray lines and reaches in Figure 4). At the network scale, the spatial distribution of disconnected reaches is nearly identical for all scenarios. Analyzing longitudinal patterns of disconnectivity along the Da River indicates that disconnectivity is mainly related to large local grain sizes which are most abundant in the upper (900–850 km) and the upper middle reaches (520–700 km) of the Da-River. This becomes evident comparing the sediment trajectories of scenario 1 and 3 (Figures 4a and 4b). Large grain sizes (i.e., gravel-cobble size) are deposited within few reaches, because of locally insufficient energy to transport them further downstream. The transport of finer sediment fractions through reaches where large sediment fractions are deposited is unimpaired for either scenario. CASCADE locates the specific edges where a sediment cascades is interrupted. This information reveals bottlenecks for sediment connectivity. In these bottlenecks a high number of cascades is interrupted (Figure 5 shows edges in which at least five cascades are interrupted). CASCADE also identifies the mechanisms for disconnectivity. Hence, if a cascade is interrupted because of a local hydro-morphologic control (equation (13), case a), or because of competition (equation (13), case b). We use scenario 3 for this analysis as the mechanisms for disconnectivity can be distinguished more clearly. Under scenario 3, all cascades could connect to a defined end-point without competition. That end-point is either the basin outlet, or an edge where a cascade's grain size cannot be entrained, and which can be identified *a-priori* using equation (13). In turn, cascades that are interrupted before their end-point are interrupted because of competition.

We find that local morphologic controls create bottlenecks where multiple cascades from smaller tributary convey larger grain sizes that cannot be entrained in the main river channel (Figure 5, red squares). Competition creates instead bottlenecks at the major confluences, with the number of disconnected cascades being proportional to the size of the confluence (Figure 5, blue circles). This indicates that competition is an additional switching mechanism that controls especially at tributary confluences which sources connect to the downstream river network.

5.4. Validation and Sensitivity Analysis

5.4.1. Comparing CASCADE Sediment Flux to Observations

As a preliminary validation we compare modeled bed-load fluxes derived from equation (17) to available observations. Total suspended solids (TSS) observations are available for 3 gauging stations in the river network (Figure 2). In average, predicted bed-load flux at these station was 2.2 $\pm$ 0.75% of observed TSS (Figure 6). These values are within the values of bed-load/TSS ratios (2–40%) observed for major sandy rivers worldwide [*Turowski et al.*, 2010]. Values are also within the range of estimates for the Mekong River, reflecting a river in a relatively similar geologic and climatic setting (1–3%) [*Bravard et al.*, 2014]. On the network scale, scenario 2 resulted in the highest sediment fluxes. Mean Θ_e for all 2123 edges was 2.1×10^9 kg yr^{-1} for scenario 1, 4.0×10^9 kg yr^{-1} for scenario 2, and 9.2×10^8 kg yr^{-1} for scenario 3. The difference in mean sediment fluxes was only significant between scenario 2 and 3 ($p=0.0015$, t-test with sample size 2123). The predicted median grain size diameter in the main river stem (Strahler Order >5) was 1.3 mm, and hence around four times the value reported by *Vinh et al.* [2014] (0.35 mm). These results indicate that the assumptions behind CASCADE are a reasonable approximation to sediment transport processes, at least in the major river channels where some data are available.

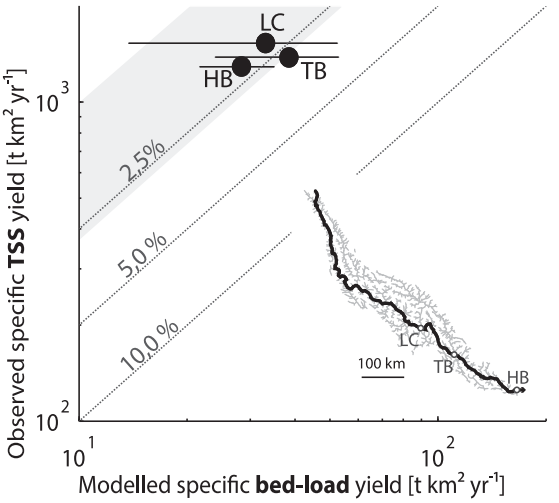

Figure 6. Comparing CASCADE results to available sediment transport calculations. Letters indicate the name of sediment gauging stations (see Figure 2). Dots represent the mean modeled value for each gauging station. Horizontal error bars represent the range of values predicted at a station for the 3 scenarios. Diagonal lines indicate bed-load/TSS ratios. The shaded area indicates the TSS/bed-load ratios reported for the Mekong (1–3%) [*Bravard et al*., 2014].

5.4.2. Toward a Networks Scale Sensitivity Analysis

In this section, we provide some insights into CASCADE sensitivity. We focus for now on the grain size of sources (d_{ς}) and use scenario 3 for the analysis. We selected d_{ς} for the sensitivity analysis for four reasons. First, d_{ς} is a direct function of local hydro-morphologic properties because of the proposed method for estimating d_{ς}. Analysing model sensitivity to d_{ς} therefore allows evaluating model sensitivity to measurement errors in hydraulic and morphometric parameters, e.g., in gradient. Measurement errors in gradient relate, in turn, to low input data resolution, or the used reach length (e.g., shorter reaches might capture a higher degree of local variability in gradient and result in steeper gradient values). Second, d_{ς} directly impacts the sediment supply from sources (equation (22)). Third, sediment inputs determine the competitiveness of a sediment cascade under scenario 3. Therefore, this analysis captures multiple aspects of model and parameter uncertainty. Fourth, the calculation of d_{ς} assumes that there is an equilibrium between bed shear stress and the grain size of a source. This assumption might not hold in many cases. For example, where mass-movements supply above-equilibrium grain sizes, or hillslope processes supply below-equilibrium grain sizes to the channel. We perturbed the grain size d_{ς} of each source by multiplying the original d_{ς} with a perturbance factor Φ_{ς} that represents deviation of the actual d_{ς} from the local equilibrium grain size because of the above mentioned mechanisms. We created four versions of Φ_{ς}. v1 ranged from 1 to 10 (0–1000% perturbance), hence d_{ς} was increased for all sources. v2 ranged from 0.1 to 10 (−90 to 1000% perturbance), d_{ς} was increased and decreased for an equal number of sources. v3 ranged from 0.1 to 1 (−90 to 0% perturbance), hence d_{ς} was decreased for all sources. v4 also ranged from 0.1 to 1, but d_{ς} was only decreased for 50% of the sources. For each version we analyzed the sediment trajectories along the main stem of the Da River. Results are shown in Figure 7. Figures 7a, 7c, 7e, and 7g visualize the probability distribution and the spatial pattern of Φ_{ς} for v1–v4. Figures 7b, 7d, 7f, 7h show the resulting sediment trajectories along the main stem of the Da River (analog to the information shown in Figure 4).

The results of this analysis indicate how disturbing the model initialization may affect the previously discussed large-scale patterns of sediment connectivity derived from CASCADE. A major network scale increase in grain sizes (v1, Figures 7a and 7b) leads to the disappearance of the clear upstream-downstream deposition pattern and a strong initial deposition along most cascades. Nevertheless, there are few cascades that are disconnected from the basin outlet (grey lines in Figure 7b). The low number of disconnected cascades can be related to a general decrease in the competitiveness of cascades because all cascades transport larger grain sizes. Under v2, with randomly increased and decreased source grain sizes, there are clearly more disconnected cascades (Figure 7d). This is because cascades with increased d_{ς} are in competition with cascades with decreased d_{ς}. Cascades reaching the basin outlet develop a continuous downstream deposition pattern. Sediment trajectories form a clear structure of different bands that are separated at tributary confluences. Nevertheless, the bands are more sparse in comparison to the original result (Figure 4b), because some sources within the bands are disconnected or experience strong deposition. This is evident in comparison to v3 (Figure 7f), for which bands are more compact. Otherwise, the observed pattern for v3 is very similar to the pattern for the original scenario 3 (Figure 4b). All cascades receive a higher sediment input, but are accordingly more competitive. Decreasing d_{ς} randomly for only some cascades (v4) provides further clarification for the functioning of the CASCADE approach (Figures 7g and 7h). Using the current parameterization, sediment sources in steep, mountainous reaches will provide larger grain sizes. This limits the input from these sources and makes them less competitive. For example,

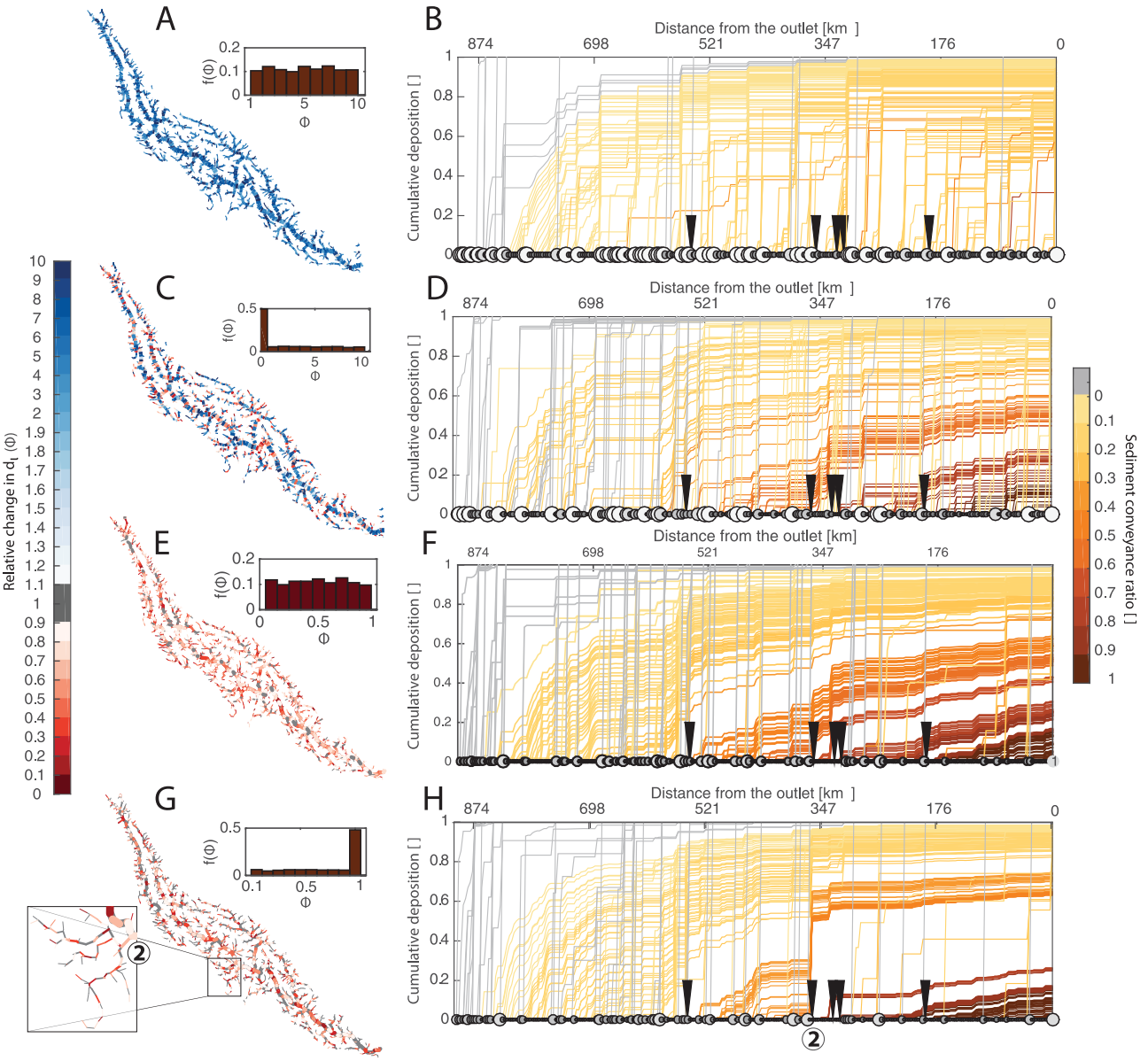

Figure 7. Analyzing the sensitivity of deposition trajectories to source grain size d_ς. The right colorbar indicates the perturbance factor (Φ) of grain size in comparison to the original values. (a, c, e, g) The spatial distribution of Φ is displayed; small histograms show the probability distribution of Φ. (b, d, f, h) Visualization of the resulting sediment trajectories. Black triangles mark tributary confluences, the point size on the x-axis indicates source grain d_ς.

tributary 2 contains the fewest sources with sandy grain size among the five major tributaries (Figure 8). This indicates that tributary 2 is the steepest of the five major tributaries. Nevertheless, tributary 2 already had a clear impact on sediment trajectories along the main channel for the original scenario 3 (Figure 4b). Applying $\Phi(v4)$ strongly decreased d_ς for some sources in tributary 2 (cutout in Figure 7g). Decreasing d_ς then increased the sediment output from this tributary by an order of magnitude (from 4.1 $\times 10^4$ tons/yr to 5.4 $\times$ 10^5 tons/yr). Sediment cascades which begin upstream of the confluence of tributary 2 now experience a much more emphasized deposition at the confluence (Figure 7h, km 360). Yet, the d_ς of sediment cascades from tributary 2 are still too large to be transported far downstream along the main stem. Therefore, the high deposition at tributary 2 reduces the competition for more downstream cascades, making them deliver sediment to the basin outlet more effectively (compare Figures 7f and 7h, downstream of km 360).

To conclude, this section provides first some evidence for the consistency of the CASCADE with regard to its reaction to changing grain sizes (e.g., larger grain sizes increase initial deposition, higher tributary inputs

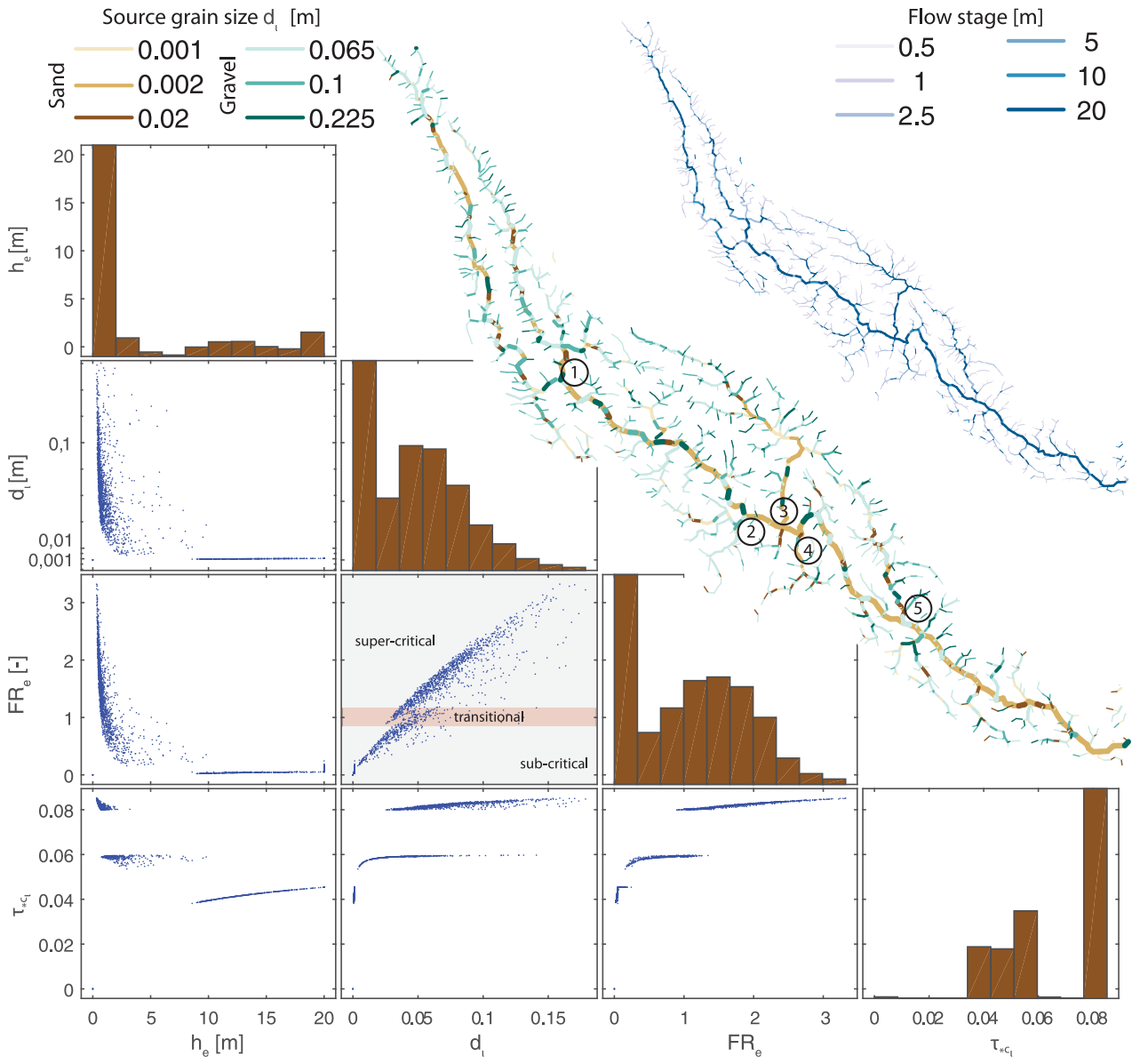

Figure 8. Correlation and frequency distribution for key hydraulic parameters (scatter plots) and the spatial pattern of derived characteristic grain sizes and flow stages (top plots). Numbers indicate main tributaries (Ad $>$ 2500 km^2). Histograms in the diagonal of the scatter matrix indicate the frequency distribution of the respective variables. The Froude Number, $Fr = v/\sqrt{g * h}$, was calculated to epitomize local hydraulic conditions. All hydraulic parameters and the flow stage plot represent hydraulic conditions at 1.5 year discharge.

increase competition along the main channel). Second, there is some evidence that the presented model results are valid for a wide range of parameterizations. The general pattern of sediment trajectories under scenario 3 collapses only if the grain size in the main stem is massively increased, changing the main stem from a sand (68% of sources deliver a $d_{\varsigma} < 2$ mm in the original parameterization) to a gravel dominated river (5% of sources deliver a $d_{\varsigma} < 2$ mm for $\Phi(v1)$).

6. Discussion

The CASCADE modeling framework quantifies network sediment connectivity by explicitly tracing sediment cascades from sources to all connected sinks. We applied CASCADE to a large river network and present the connectivity information that can be derived using very limited input data. We provide some indication for how CASCADE enables analyzes of complex sediment transport processes and connectivity on the network

scale. This novel connectivity information clarifies the internal functioning of the CASCADE model, allows assessment of its limitations, and its sensitivity to internal and external boundary conditions. Finally, we discuss how this new information could support river science and management. Nearly all analyses presented in this article rely on multiple domains of sediment connectivity (location of sources, source-specific flux, and delivered grain sizes). The ability of CASCADE to provide this information enabled us to reproduce often observed phenomena such as preferential connectivity that can hardly be reproduced with common sediment modeling approaches.

For example, field evidence points out the role of local hydro-morphologic controls that act as grain size depending switches that either facilitate or disrupt sediment connectivity [*Fryirs et al*., 2007a,b]. CASCADE can readily locate such switches by identifying where a specific sediment cascade is disconnected from the downstream river network. Additionally, our results extend the analysis of sediment switches. Not only local morphologic controls but also the continuous deposition along a sediment cascade can result in disconnectivity for specific cascades at specific locations. Yet, these switches are potentially variable in space. For example, if some cascades are disconnected by the construction of a reservoir, more downstream sources can become better connected to the remainder of the river network because competition is reduced. Hence, CASCADE points out permanent, physical disconnections but also partial or transient disconnections that can be connected under the right environmental circumstances, or as reaction to human interventions [*Jain and Tandon*, 2010].

Sediment trajectories provide source specific information on the fate of sediment but also allow reproducing large scale patterns of sediment connectivity. These spatial patterns can be compared to some well-established concepts of network connectivity. Sediment trajectories obtained using a supply driven competition factor (scenario 3) closely match the observation of *Arnaud-Fassetta* [2004], who observed that the contribution of an upstream source to a downstream sink decreases with increasing distance between both. Yet, observations with this regard are equivocal. Results of *Clift et al*. [2004] for the Mekong indicate that preferential connectivity, similar to the pattern observed under scenario 1, can be relevant even in very large river systems. CASCADE also allows quantification of the impact of local confluence effects on network scale sediment connectivity. With regard to confluence effects, scenario 3 results in connectivity patterns that are in close accordance with empirical observations. For example, *Rice et al*. [2006] and *Benda et al*. [2004a, 2004b] document how tributaries effect main channel morphology and sediment connectivity. The magnitude of these confluence effects strongly related to the fraction of main channel transport versus tributary inputs. Such a pattern is reproduced mainly under scenario 3. The sensitivity analysis provided evidence that CASCADE captures the correlation between main-channel connectivity and tributary inputs. The sensitivity analysis also indicates that observed patterns strongly relate to the transported grain sizes, and that the clear network scale pattern observed for scenario 3 mainly emerges for sand-bed rivers. Based on the results and the available information, we cannot state that any of the three scenarios is *per-se* more appropriate. Scenario selection should instead be based on comparing CASCADE results to, even sparse or broad, empirical observations for the river system under study. Yet, we propose that Scenario 3 can be a good starting point for model initialization, as it was able to reproduce some key traits of connectivity for the network under study. Analyzing the sensitivity indicate that these general observations are relatively insensitive to initial conditions.

Obviously, the presented modeling framework is not conceived as a process-based hydro-dynamic sediment transport model for detailed studies of coupled sediment transport and river morphologic processes. So far, CASCADE does not consider a morphologic adaptation of the river network to sediment inputs, e.g., in terms of gradient. The fluvial network presents a static template along which various bed-load fractions are routed and their interaction can be studied. The proposed initialization of grain sizes based on remote sensing data is a highly simplified attempt to address the widespread lack of sedimentologic data with a quantitative, spatially continuous, and globally applicable approach. Network scale source initialization will also improve with time-series of high-resolution fluvial data sets on network or regional scales [*Bizzi et al*., 2016]. Such data sets will progress automated identification of, e.g., relevant sites of bank erosion or in-channel stores of sediment that can act as additional sources. In the future, there are relevant links between the automated, object-based structural mapping of fluvial forms [*Demarchi et al*., 2016] and connectivity modeling. Information on local sediment connectivity can provide a stronger link between structural mapping of fluvial forms and fluvial processes. In turn, a detailed structural mapping can greatly support model

initialization and validation of a connectivity model, e.g., with regard to identifying active channel margins, floodplains or in-channel landforms [*Fryirs et al*., 2016] that can serve as sediment sources or sinks during overbank flow events.

There are multiple aspects of network scale sediment transport processes that should be included into future versions of CASCADE. Attrition of larger grains [*Parker*, 1991] could increase the connectivity of upstream gravel and cobble sources, while demobilization on floodplains could create additional sinks for smaller grain size fractions. Through its multigraph structure, CASCADE can be easily expanded to consider additional connected transfer processes. Enlarging the scope from the network to the landscape scale could be achieved by adding additional sediment cascades that explicitly represent hillslope processes [e.g., *Heckmann and Schwanghart*, 2013] or the transfer from active sediment stores [*Tunnicliffe et al*., 2012; *Tunnicliffe and Church*, 2011]. Additionally, cascades can be added to represent not only the routing of bed-load, but also of finer, suspended load fractions.

CASCADE should, above all, be considered as a flexible, exploratory tool to project the impact of local controls, conceptualizations, and empiric observations (which are, e.g., the basis of most sediment transport formulations) onto all scales and domains of sediment connectivity for a real river system [cf. *Bracken et al*., 2015; *Brierley et al*., 2006]. CASCADE will also support transferring newly available fluvial data sets into physically based indicators for the connected functioning of fluvial systems. Second, it is increasingly evident that the long acknowledged complexity in sediment and, specifically, bed-load transport processes [*Walling*, 1983] is still missing from most numerical, or conceptual sediment management approaches [*Fryirs*, 2013]. At the same time, information on sediment sources and stores is largely absent even in better studied river basins [e.g., *Walling*, 2008]. CASCADE adds a relevant component with this regard in comparison to previous approaches, which is relevant for both knowledge discovery and river management. *Reid and Brierley* [2015] point out that the local sensitivity of a river to change is a function of both local morphologic controls and upstream sediment inputs. The ability of CASCADE to identify the sediment sources for a specific reach can help to identify most vulnerable or resilient reaches, and the timescales over which upstream changes will impact downstream reaches. With this regard, CASCADE supports deriving spatially explicit indicators for fluvial resilience that embalm both the response time and the magnitude of downstream change to an upstream disturbance. Current models for management oriented, basin scale sediment assessments are computationally effective but rely often on scarce empirical observations [*Kondolf et al*., 2014; *Wild and Loucks*, 2014]. In comparison, CASCADE greatly increases the fidelity with which sediment transport processes can be reproduced on the network scale. A single CASCADE run can only provide a first order estimate of network scale sediment transport processes without more detailed input data. Nevertheless, CASCADE is an effective, process-related screening model to analyze a high number of different scenarios or parameterizations. Soon, CASCADE will also be made publicly available.

CASCADE covers the most relevant process domains of connectivity [*Bracken et al*., 2015], namely detachment, transport, and deposition of each grain size fraction. CASCADE also provides new capabilities with regard to visualization, interpretation, and quantification of multiscale sediment source-sink relations. With this regard, CASCADE can considerably increase our ability to analyze connected sediment transfers on the river network or basin scales, a prerequisite to foresee and communicate human impacts on sediment connectivity and related ecosystem functions and services [*Fryirs*, 2013].

7. Conclusion

The CASCADE (**CA**tchment **S**ediment **C**onnectivity **A**nd **DE**livery) modeling framework is a novel approach to quantify sediment deliveries between all sediment sources and sinks in large fluvial networks. The major novelty is that CASCADE describes the transport of sediment from each specific source as an individual cascading process. In this paper, we demonstrate how the resulting information can be used to study most relevant domains of sediment connectivity over multiple spatio-temporal scales. We exemplify the application of CASCADE and the analysis of the resulting connectivity information for a major basin in SE Asia. Specifically, we used CASCADE to study the connectivity of a single reach to the contributing river network, to analyze the fate of sediment from manifold sources, to identify network patterns of connectivity, and to identify bottlenecks for sediment connectivity. In this article, the parameterization of CASCADE relied heavily on medium-resolution remote sensing data. Yet, this application demonstrated an implementation

strategy that makes CASCADE applicable as an effective screening model for the very large, poorly monitored river network under study. Nevertheless, CASCADE can be readily adapted to assimilate additional information and to include further relevant processes. This encourages us to propose CASCADE as a powerful computational tool to derive multiscale indicators for network sediment connectivity with applications in both river science and management.

Appendix A: The Hydrodynamic Solver

The derivation of hydraulic conditions in an edge for a given flow is based on the Manning-Strickler formula for uniform, open-channel flow [*Strickler*, 1923]. Flow velocity is calculated as

$$v_e = \frac{1}{n_{Str}} \cdot {R_{h_e}}^{2/3} \cdot {I_e}^{0.5}, \tag{A1}$$

where n_{Str} is the Manning-Strickler friction coefficient. Here we use $\frac{1}{n_{Str}} = 35$ as typical value of natural streams [*Chow*, 1959]. R_{h_e} is the hydraulic radius defined as

$$R_{h_e} = \frac{h_e \cdot W_{AC_e}}{2h_e + W_{AC_e}}. \tag{A2}$$

We assume that river channels are rectangular in all reaches and for all flow stages. We rewrite v_e as flow per channel cross-sectional area

$$v_e = \frac{Q_e}{W_{AC_e} \cdot h_e}, \tag{A3}$$

hence

$$Q_e = \frac{1}{n_{Str}} \left(\frac{h_e \cdot W_{AC_e}}{2h_e + W_{AC_e}} \right)^{2/3} \cdot I_e^{0.5} \cdot W_{AC_e} \cdot h_e. \tag{A4}$$

There is no explicit solution for equation (A4) but Q_e is a function of h_e only. Therefore we transfer equation (A4) into

$$Q_{calc_e} = \frac{1}{n_{Str}} \left(\frac{h_e \cdot W_{AC_e}}{2h_e + W_{AC_e}} \right)^{2/3} \cdot I_e^{0.5} \cdot W_{AC_e} \cdot h_{est_e}. \tag{A5}$$

Q_{calc_e} is the value of Q_e calculated by using an estimated value of h_e (h_{est_e}). We apply a nonlinear minimization algorithm to identify h_e such that

$$h_e = \min_{h_{est_e}} |Q_e - Q_{calc_e}|. \tag{A6}$$

From equation (A3) it is evident that the estimation of h_e allows to calculate v_e. The selection of an initial estimate of h_e in equation (A6) is relevant for the solving procedure. We used a hydraulic geometry relation

$$h_{est_e} = {Q_e}^{0.289} \cdot {I_e}^{-0.035} \tag{A7}$$

for that purpose [*Huang et al.*, 2002].

Appendix B: Deriving Source Grain Size Estimates

We assumed that only the largest fractions of the grain size mixture in a reach (e.g., $d > d_{90}$) are not entrained under bankfull flow conditions. We approximate the size of at this fraction through

$$d_{90_\varsigma} = \frac{I_e \cdot h_e(Q_{1.5})}{R \cdot {\tau_{*c_e}}^{\varsigma}} \tag{B1}$$

Shields [1936], where ${\tau_{*c_e}}^{\varsigma}$ is the critical shields parameter for the entrainment of d_ς in e. The transport rate of d_{90_ς} would accordingly be negligible according to B1 even for bankfull flow conditions. Therefore, we convert d_{90_ς} into the source grain sizes

$$d_{\varsigma} = \frac{d_{90_{\varsigma}}}{2.1}, \tag{B2}$$

similar to the conversion from a d_{90} to a d_{50} [*Bray*, 1987].

$\tau_{*c_e}{}^{\varsigma}$ is crucial parameter in equation (B1). $\tau_{*c_e}{}^{\varsigma}$ is not constant but a function of the grain Reynolds Number [see e.g., *Parker et al*., 2003; *Buffington and Montgomery*, 1997] which is defined as:

$$Re_{p_{\varsigma}} = \frac{\sqrt{R \cdot g \cdot d_{90_{\varsigma}}}}{\nu}. \tag{B3}$$

Brownlie [1982] proposes to calculate

$$\tau_{*c_{\varsigma}} = 0.22 Re_{p_{\varsigma}}^{-0.6} + 0.06 \cdot 10^{-7.7 \cdot Re_{p_{\varsigma}}^{-0.6}}. \tag{B4}$$

Besides, $\tau_{*c_{\varsigma}}$ increases strongly with increasing slope as the proportion between flow stage and local grain size decreases [e.g., *Lamb et al*., 2008]. Neglecting this effect yields very large $d_{90_{\varsigma}}$ from equation (B1). *Suszka* [1991] proposed that equation (B4) holds only where $h/d_{90} > 10$. For streams where this condition is exceeded for $h = h_{e(Q_{1.5})}$ we implemented therefore the formulation proposed by *Suszka* [1991]. The final calculation routine was

$$\tau_{*ce}{}^{\varsigma} = \begin{cases} 0.22 Re_{p_{\varsigma}}{}^{-0.6} + 0.06 \cdot 10^{-7.7 \cdot Re_{p_{\varsigma}}{}^{-0.6}}, \\ \text{if } h_e(Q_{1.5})/d_{90_{\varsigma}} > 10, \\ 0.0851 \cdot \left(\frac{h_e}{d_{90_{\varsigma}}}\right)^{-0.0261}, \text{else}. \end{cases} \tag{B5}$$

From equations (B3)–(B5) it is evident that there is no analytic solution for the calculation of $d_{90_{\varsigma}}$. This is because the calculation of $d_{90_{\varsigma}}$ (equation (B1)) is a function of the critical Shields parameter $\tau_{*c_{\varsigma}}$, which is in turn a function of $d_{90_{\varsigma}}$ (equations (B3)–(B5)).

We approach this problem by first assuming fully turbulent flow conditions and $\tau_{*c_{\varsigma}}$ takes a constant value of 0.047 [*Wong and Parker*, 2006]. This value is used to solve equation (B1) and to derive a first estimate of $d_{90_{\varsigma}}$ denoted as $d^*_{90_{\varsigma}}$. Equations (B3)–(B5) are subsequently solved using $d^*_{90_{\varsigma}}$. The resulting $\tau_{*c_{\varsigma}}(d_{90_{\varsigma}}{}^*)$ is then used to calculate d_{ς}.

Obviously, the proposed method is subject to a number of assumptions and sources of uncertainty. Assumptions are specifically:

1. We assume steady flow throughout the basin and for all flows stages replacing the energy slope with the gradient measured from the DEM. Channel geometry is rectangular for all channels.
2. We use a constant friction factor derived from literature. The friction-factor in CASCADE is independent of grain size and does not consider for the presence of bed-forms (e.g., bed dunes) or vegetation.
3. The estimation of local grain sizes from the critical shear stress is a rough approximation of the complex inter-dependencies of incipient sediment motion and, e.g., grain size mixture properties, small scale sedimentologic properties, or local morphology [e.g., *Lamb et al*., 2008; *Wilcock*, 1993; *Kirchner et al*., 1990].

Appendix C: Network-Scale Distribution of Hydraulic Parameters and Grain Sizes

Figure 8 displays the key hydraulic characteristics for the river basin that were derived using the hydraulic solver. All variables are shown for bankfull ($Q_{1.5_e}$) flow conditions. As additional indicator for local hydraulic conditions we calculated the Froude Number $FR_e = v_e/\sqrt{g \cdot h_e}$.

The probability distribution of flow stages, $h_e(Q_{1.5})$, is strongly left skewed with a probability maximum of 0–2 m. These observations occur in small reaches. These reaches cover a wide range of slope conditions, as FR_e for these reaches spans both the sub- and supercritical range. Supercritical flow conditions occur nearly exclusively within this group of reaches. As a result of the wide range of hydraulic conditions, these small reaches feature d_{ς} from sand to cobble size. It is also for these reaches that the correction of τ_{*c} (equation (B5)) takes effect. τ_{*c} is increased for the majority of these reaches (see distribution of τ_{*c}). This increase takes effect only for d_{ς} in the gravel or cobble range (see scatter of τ_{*c} versus d_{ς}) and hence we can deduce that the majority of reaches with low h_e feature a gravel or cobble bed composition.

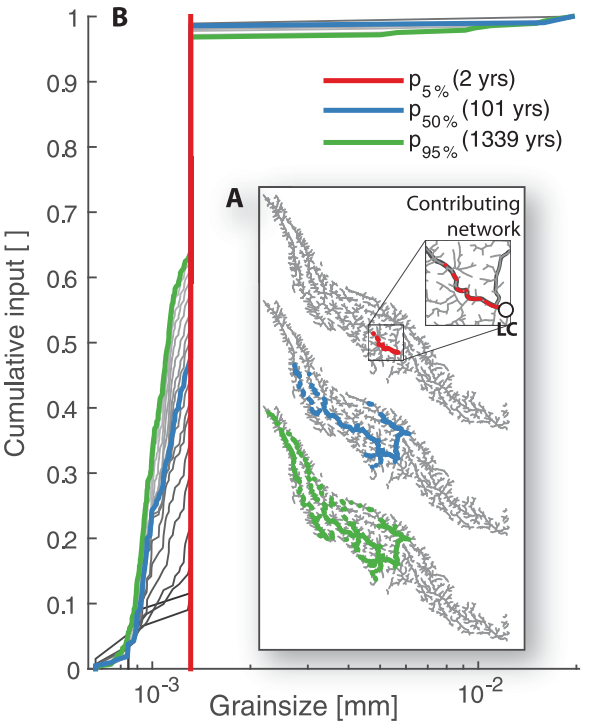

Figure 9. Reach connectivity for scenario 2. (a) Source areas and (b) fraction of input belonging to a certain grain size class for different percentiles of connection time.

There is a major group of reaches with medium-high $h_e(Q_{1.5})$ (5 - 20 m) that exhibit a homogeneous hydraulic behavior (very low FR_e). This relates to the peak in grain size distribution for small grain sizes ($d_\varsigma < 0.02$ m). This group contains the major sandy reaches ($d_\varsigma < 0.001$ m) and the conditions at the water-sediment boundary range from hydraulically smooth (medium τ_{*c}), to transitional (low τ_{*c}) (see scatter of τ_{*c} versus d_ς).

In general, there is a strong correlation between hydraulic parameters (FR_e, τ_{*c}) and d_ς. Nevertheless, the procedure clearly distinguishes between sub- and super-critical flow conditions. Large grain sizes ($d_\varsigma > 0.05$ m) are predicted to occur only under supercritical and small grain sizes ($d_\varsigma < 0.02$ m) only under subcritical flow conditions with some overlap under transitional hydraulic regimes (see scatter d_ς versus Fr_e).

The spatial distribution of hydraulic parameters is reasonable (Figure 8, top right). Here we display flow stage $h_{e(Q_{1.5})}$ and grain size d_ς. Both are key parameters in the hydraulic calculations. As expected, $h_e(Q_{1.5})$ increases with increasing A_d. The spatial distribution of d_ς is more heterogeneous. Main channel sources exhibit a sandy d_ς but with an increasing number of sources supplying coarser material in the upper parts of the basin and the major tributaries. Sources in smaller tributaries and headwaters feature a d_ς in the gravel/cobble range. Noticeably, sources in tributary 3 supply predominantly sandy sediment.

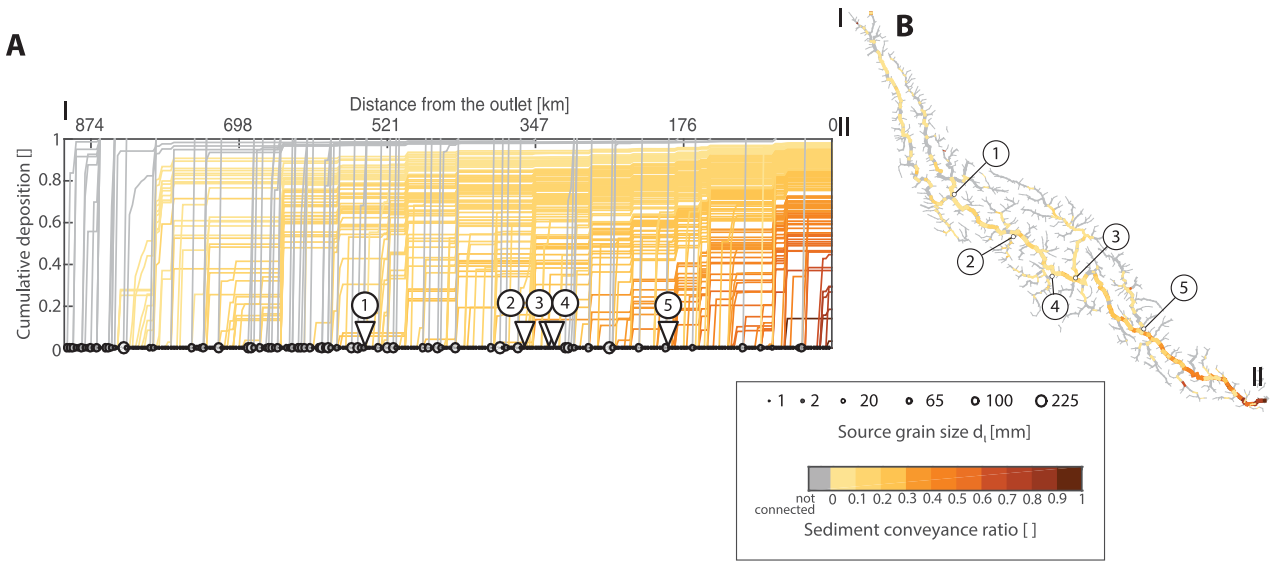

Figure 10. Network connectivity for scenario 2. (a) Deposition trajectories along the main stem of the Da River. Dots indicate the source grain size d_ς transported along each cascade. Numbers and triangles indicate the location of major tributaries ($A_D > 2500 km^2$, see Figure 8). (b) The sediment conveyance ratio is mapped throughout the river basin.

Appendix D: Connectivity Under Scenario 2

This section reports findings for scenario 2 (not presented in the main article). Figure 9 illustrates the results for connectivity analysis for the single reach under study (compare section 5.1). Observations are similar to scenario 3. Connectivity is mainly established along the main river for small connection times but the source areas are less connected than under scenario 3. We observe little preferential connectivity and upstream reaches connect only for longer connection times. Grain sizes are fining with increasing connection times.

Figure 10 presents the sediment redistribution along the main stem and on the network scale (compare section 5.2). Scenario 2 results in an intermediate situation between scenario 1 and 3. Most sediment cascades experience strong initial deposition, and tributaries have little influence on sediment redistribution along the main stem. Still, there is a clear upstream-downstream gradient in sediment delivery both along the main stream and on the network scale.

Notation

A_D	Drainage Area, km^2.
A_e	Set of edge attributes.
A_x	Cross-sectional area of sediment transport, m^2.
a	Cardinality of A_e.
a	Parameter $A_D - Q_{1.5}$ relation.
b	Parameter $A_D - Q_{1.5}$ relation.
C_f	Friction factor.
d	Grain size, m.
d_{50}	Median grain size, m.
E	Full set of edges in G.
e	Specific edge in E.
e	Cardinality of E
F	Competition Factor.
FR	Froude number.
G	River Graph.
g	Gravitational acceleration, $kg\ m\ s^{-2}$.
g	Cardinality of Γ.
h	Flow stage, m.
I	Channel gradient [$m\ m^{-1}$].
J	Hydrograph scaling factor.
L	Edge length, m.
m_{AD-W}	Parameter $A_D - W_{AC}$ relation.
N	Full set of nodes in G.
n	Cardinality of N.
n	Specific node in N.
n_{AD-W}	Parameter $A_D - W_{AC}$ relation.
n_p	Number of discharge observation within the $p - th$ discharge percentile.
n_{Str}	Manning-Strickler friction factor, $s\ m^{1/3}$.
n_{tot}	Total number of discharge observations for a reach.
p	Discharge percentile.
$\boldsymbol{Q}$	Discharge time series, $m^3\ s^{-1}$.
Q	Discharge, $m^3\ s^{-1}$.
$Q_{1.5}$	1.5 year return period discharge, $m^3\ s^{-1}$.
Q_S	Sediment Transport capacity, $kg\ yr^{-1}$.
Q_S'	Competition corrected sediment transport capacity, $kg\ yr^{-1}$.
$Q_{S,in}$	Sediment supply, $kg\ yr^{-1}$.
q_{S*}	Dim. less transport capacity.
q_S	Transport capacity per unit channel width, $m^2\ d^{-1}$.
R	Relative sediment density.

R_h	Hydraulic radius, m.
Re_p	Particle Reynolds Number.
S	Full set of sources.
s	Cardinality of S.
T	Connection time, years.
t	Residence time, years.
v	Flow velocity, m s^{-1}.
W_{AC}	Active channel width, m.
α	Parameter, Wong-Parker Sediment transport formula.
β	Parameter, Wong-Parker Sediment transport formula.
Γ	Full set of sediment cascades.
γ	specific sediment cascade in Γ.
ε	Subset of edges along a pathway κ.
Θ	Sediment flux, kg yr^{-1}.
θ	Characteristic transport depth, m.
κ	cascade pathway.
ν	Kinematic viscosity, m^2 s^{-1}.
ρ_S	Sediment density, kg m^{-3}.
ς	Specific source in S.
τ_*	Dim. less shear stress.
τ_{*c}	Dim. less critical shear stress.
Ω	Identifier of basin outlet node

Acknowledgments

Data used in this paper were partially collected under the project IMRR (Integrated and sustainable water Management of Red Thai Binh Rivers System in changing climate), funded by the Italian Ministry of Foreign Affairs (Delibera n. 142 del 8 Novembre 2010). Rafael Schmitt was supported by a Ph.D. scholarship of the German National Academic Foundation. We thank Dr. Gary Brierley, Jonathan A. Czuba, and an anonymous reviewer whose comments helped to better frame and improve this paper significantly. Please contact the author (RS) for obtaining specific data or model results.

References

Andrews, E. D. (1983), Entrainment of gravel from naturally sorted riverbed material, *Geol. Soc. Am. Bull.*, *94*(10), 1225–1231, doi:10.1130/0016-7606(1983)94¡1225:EOGFNS¿2.0.CO;2.

Arnaud-Fassetta, G. (2004), The upper Rhône delta sedimentary record in the Arles-Piton core: Analysis of delta-plain subenvironments, avulsion frequency, aggradation rate and origin of sediment yield, *Geogr. Ann., Ser. A*, *86*(4), 367–383, doi:10.1111/j.0435-3676.2004.00238.x.

Bechtol, V., and L. Laurian (2005), Restoring straightened rivers for sustainable flood mitigation, *Disaster Prev. Manage. Int. J.*, *14*(1), 6–19, doi:10.1108/09653560510583806.

Benda, L., and T. Dunne (1997), Stochastic forcing of sediment routing and storage in channel networks, *Water Resour. Res.*, *33*(12), 2865–2880, doi:10.1029/97WR02387.

Benda, L., N. L. Poff, D. Miller, T. Dunne, G. Reeves, G. Pess, and M. Pollock (2004a), The network dynamics hypothesis: How channel networks structure riverine habitats, *BioScience*, *54*(5), 413–427, doi:10.1641/0006-3568(2004)054[0413:TNDHHC]2.0.CO;2.

Benda, L., K. Andras, D. Miller, and P. Bigelow (2004b), Confluence effects in rivers: Interactions of basin scale, network geometry, and disturbance regimes, *Water Resour. Res.*, *40*, W05402, doi:10.1029/2003WR002583.

Bizzi, S., and D. N. Lerner (2016), The use of stream power as an indicator of channel sensitivity to erosion and deposition processes, *River Res. Appl.*, *31*(1), 16–27, doi:10.1002/rra.2717.

Bizzi, S., L. Demarchi, R. C. Grabowski, C. J. Weissteiner, and W. V. de Bund (2016), The use of remote sensing to characterise hydromorphological properties of European rivers, *Aquat. Sci.*, *78*, 1–14, doi:10.1007/s00027-015-0430-7.

Bracken, L. J., L. Turnbull, J. Wainwright, and P. Bogaart (2015), Sediment connectivity: A framework for understanding sediment transfer at multiple scales, *Earth Surf. Processes Landforms*, *40*, 177–188, doi:10.1002/esp.3635.

Bravard, J.-P., M. Goichot, and H. Tronchère (2014), An assessment of sediment-transport processes in the lower Mekong river based on deposit grain sizes, the CM technique and flow-energy data, *Geomorphology*, *207*, 174–189, doi:10.1016/j.geomorph.2013.11.004.

Bray, D. (1987), *A Review of Flow Resistance in Gravel Bed Rivers*, Leggi Morfologichee loro verifica del Campo, Editoriale BIOS-Cosenza, Univ. di Calabria, Cosenza, Italy.

Brierley, G., K. Fryirs, and V. Jain (2006), Landscape connectivity: The geographic basis of geomorphic applications, *Area*, *38*(2), 165–174, doi:10.1111/j.1475-4762.2006.00671.x.

Brownlie, W. R. (1982), Prediction of flow depth and sediment discharge in open channels, *Tech. Rep. Rep. KH-R-43A*, W. M. Keck Lab. of Hydraul. and Water Resour., Calif. Inst. of Technol., Pasadena.

Buffington, J. M., and D. R. Montgomery (1997), A systematic analysis of eight decades of incipient motion studies, with special reference to gravel-bedded rivers, *Water Resour. Res.*, *33*(8), 1993–2029, doi:10.1029/96WR03190.

Cheung, A. K. L., D. O'sullivan, and G. Brierley (2015), Graph-assisted landscape monitoring, *Int. J. Geogr. Inf. Sci.*, *29*(4), 580–605, doi:10.1080/13658816.2014.989856.

Chow, V. T. (1959), *Open-Channel Hydraulics*, McGraw-Hill, N. Y.

Church, M., P. Biron, A. G. Roy, and P. Ashmore (2012), *Gravel Bed Rivers: Processes, Tools, Environments*, John Wiley, Hoboken, N. J.

Clift, P. D., G. D. Layne, and J. Blusztajn (2004), Marine sedimentary evidence for monsoon strengthening, Tibetan uplift and drainage evolution in East Asia, in *Continent-Ocean Interactions in the East Asian Marginal Seas, Geophys. Monogr. Ser., 149*, edited by P. Clift et al., pp. 255–282, AGU, Washington, D. C.

Czuba, J. A., and E. Foufoula-Georgiou (2014), A network-based framework for identifying potential synchronizations and amplifications of sediment delivery in river basins, *Water Resour. Res.*, *50*, 3826–3851, doi:10.1002/2013WR014227.

Czuba, J. A., and E. Foufoula-Georgiou (2015), Dynamic connectivity in a fluvial network for identifying hotspots of geomorphic change, *Water Resour. Res.*, *51*, 1401–1421, doi:10.1002/2014WR016139.
Demarchi, L., S. Bizzi, and H. Piégay (2016), Hierarchical object-based mapping of riverscape units and in-stream mesohabitats using LiDAR and VHR imagery, *Remote Sens.*, *8*(2), 97, doi:10.3390/rs8020097.
Dietrich, W. E., J. W. Kirchner, H. Ikeda, and F. Iseya (1989), Sediment supply and the development of the coarse surface layer in gravel-bedded rivers, *Nature*, *340*(6230), 215–217, doi:10.1038/340215a0.
Dijkstra, E. W. (1959), A note on two problems in connexion with graphs, *Numer. Math.*, *1*(1), 269–271.
Engelund, F., and E. Hansen (1967), *A Monograph on Sediment Transport in Alluvial Streams*, Tekniskforlag, Copenhagen.
Fryirs, K. (2013), (Dis)connectivity in catchment sediment cascades: A fresh look at the sediment delivery problem, *Earth Surf. Processes Landforms*, *38*(1), 30–46, doi:10.1002/esp.3242.
Fryirs, K. A., G. J. Brierley, N. J. Preston, and M. Kasai (2007a), Buffers, barriers and blankets: The (dis)connectivity of catchment-scale sediment cascades, *Catena*, *70*(1), 49–67, doi:10.1016/j.catena.2006.07.007.
Fryirs, K. A., G. J. Brierley, N. J. Preston, and J. Spencer (2007b), Catchment-scale (dis)connectivity in sediment flux in the upper Hunter catchment, new south wales, Australia, *Geomorphology*, *84*(3–4), 297–316, doi:10.1016/j.geomorph.2006.01.044.
Fryirs, K. A., J. M. Wheaton, and G. J. Brierley (2016), An approach for measuring confinement and assessing the influence of valley setting on river forms and processes, *Earth Surf. Processes Landforms*, doi:10.1002/esp.3893.
Gatto, M., L. Mari, E. Bertuzzo, R. Casagrandi, L. Righetto, I. Rodriguez-Iturbe, and A. Rinaldo (2013), Spatially explicit conditions for waterborne pathogen invasion, *Am. Nat.*, *182*(3), 328–346, doi:10.1086/671258.
Habersack, H., D. Haspel, and M. Kondolf (2014), Large rivers in the anthropocene: Insights and tools for understanding climatic, land use, and reservoir influences, *Water Resour. Res.*, *50*, 3641–3646, doi:10.1002/2013WR014731.
Heckmann, T., and W. Schwanghart (2013), Geomorphic coupling and sediment connectivity in an alpine catchment — exploring sediment cascades using graph theory, *Geomorphology*, *182*, 89–103, doi:10.1016/j.geomorph.2012.10.033.
Heckmann, T., W. Schwanghart, and J. D. Phillips (2015), Graph theory—Recent developments of its application in geomorphology, *Geomorphology*, *243*, 130–146, doi:10.1016/j.geomorph.2014.12.024.
Hooke, J. (2003), Coarse sediment connectivity in river channel systems: A conceptual framework and methodology, *Geomorphology*, *56*(1–2), 79–94, doi:10.1016/S0169-555X(03)00047-3.
Hsu, I., and F. J. Holly (1992), Conceptual bed-load transport model and verification for sediment mixtures, *J. Hydraul. Eng.*, *118*(8), 1135–1152, doi:10.1061/(ASCE)0733-9429(1992)118:8(1135).
Huang, H. Q., G. C. Nanson, and I. D. Fagan (2002), Hydraulic geometry of straight alluvial channels and the principle of least action, *J. Hydraul. Res.*, *40*(2), 153–160, doi:10.1080/00221680209499858.
Jain, V., and S. K. Tandon (2010), Conceptual assessment of (dis)connectivity and its application to the Ganga River dispersal system, *Geomorphology*, *118*(3–4), 349–358, doi:10.1016/j.geomorph.2010.02.002.
Kirchner, J. W., W. E. Dietrich, F. Iseya, and H. Ikeda (1990), The variability of critical shear stress, friction angle, and grain protrusion in water-worked sediments, *Sedimentology*, *37*(4), 647–672, doi:10.1111/j.1365-3091.1990.tb00627.x.
Knighton, D. (1984), *Fluvial Forms and Processes*, Edward Arnold, London, U. K.
Kondolf, G., Z. Rubin, and J. Minear (2014), Dams on the Mekong: Cumulative sediment starvation, *Water Resour. Res.*, *50*, 5158–5169, doi:10.1002/2013WR014651.
Lamb, M. P., W. E. Dietrich, and J. G. Venditti (2008), Is the critical shields stress for incipient sediment motion dependent on channel-bed slope?, *J. Geophys. Res.*, *113*, F02008, doi:10.1029/2007JF000831.
Le, T. P. Q., J. Garnier, B. Gilles, T. Sylvain, and C. Van Minh (2007), The changing flow regime and sediment load of the Red River, Viet Nam, *J. Hydrol.*, *334*(1–2), 199–214, doi:10.1016/j.jhydrol.2006.10.020.
Milliman, J. D., and R. H. Meade (1983), World-wide delivery of river sediment to the oceans, *J. Geol.*, *91*, 1–21, doi:10.1086/628741.
Molinas, A., and B. Wu (2000), Comparison of fractional bed-material load computation methods in sand-bed channels, *Earth Surf. Processes Landforms*, *25*(10), 1045–1068, doi:10.1002/1096-9837(200009)25:10¡1045::AID-ESP115¿3.0.CO;2-X.
Parker, C., C. R. Thorne, and N. J. Clifford (2015), Development of ST:REAM: A reach-based stream power balance approach for predicting alluvial river channel adjustment, *Earth Surf. Processes Landforms*, *40*(3), 403–413, doi:10.1002/esp.3641.
Parker, G. (1990), Surface-based bedload transport relation for gravel rivers, *J. Hydraul. Res.*, *28*(4), 417–436, doi:10.1080/00221689009499058.
Parker, G. (1991), Selective Sorting and Abrasion of River Gravel. I: Theory, *J. Hydraul. Eng.*, *117*(2), 131–147, doi:10.1061/(ASCE)0733-9429(1991)117:2(131).
Parker, G., C. M. Tore-Escoba, M. Ramey, and I. Beck (2003), Effect of floodwater extraction on mountain stream morphology, *J. Hydraul. Eng.*, *129*(11), 885–895.
Reid, H. E., and G. J. Brierley (2015), Assessing geomorphic sensitivity in relation to river capacity for adjustment, *Geomorphology*, *251*, 108–121, doi:10.1016/j.geomorph.2015.09.009.
Rice, S. P., R. I. Ferguson, and T. B. Hoey (2006), Tributary control of physical heterogeneity and biological diversity at river confluences, *Can. J. Fish. Aquat. Sci.*, *63*(11), 2553–2566.
Rinaldo, A., G. Botter, E. Bertuzzo, A. Uccelli, T. Settin, and M. Marani (2006), Transport at basin scales: 2. applications, *Hydrol. Earth Syst. Sci.*, *10*(1), 31–48, doi:10.5194/hess-10-31-2006.
Schmitt, R., I. Bizzi, and A. Castelletti (2014), Characterizing fluvial systems at basin scale by fuzzy signatures of hydromorphological drivers in data scarce environments, *Geomorphology*, *214*, 69–83, doi:10.1016/j.geomorph.2014.02.024.
Shields, A. (1936), *Anwendung der Ähnlichkeitsmechanik und der Turbulenzforschung auf die Geschiebebewegung*, Eigenverl. der Preußischen Versuchsanst. für Wasserbau, Berlin.
Strickler, A. (1923), *Beiträge zur Frage der Geschwindigkeitsformel und der Rauhigkeitszahlen für Ströme, Kanäle und geschlossene Leitungen. Mitteilungen des Amtes für Wasserwirtschaft*., Eidg. Amt für Wasserwirtschaft, Bern.
Suszka, L. (1991), Modification of transport rate formula for steep channels, in *Fluvial Hydraulics of Mountain Regions, Lecture Notes Earth Sci. 37*, edited by P. A. Armanini and P. G. D. Silvio, pp. 59–70, Springer, Berlin.
Sutherland, A. J. (1987), Armouring processes, in *Sediment Transport in Gravel-Bed Rivers*, edited by C. R. Thorne, J. C. Bathurst, and R. D. Hey, pp. 243–269, John Wiley, N. Y.
Tarboton, D. G., R. L. Bras, and I. Rodriguez-Iturbe (1991), On the extraction of channel networks from digital elevation data, *Hydrol. Processes*, *5*(1), 81–100.
Trush, W. J., I. M. McBain, and L. B. Leopold (2000), Attributes of an alluvial river and their relation to water policy and management, *Proc. Natl. Acad. Sci. U. S. A.*, *97*(22), 11,858–11,863, doi:10.1073/pnas.97.22.11858.

Tunnicliffe, J., M. Church, J. J. Clague, and J. K. Feathers (2012), Postglacial sediment budget of Chilliwack Valley, British Columbia, *Earth Surf. Processes Landforms*, *37*(12), 1243–1262, doi:10.1002/esp.3229.
Tunnicliffe, J. F., and M. Church (2011), Scale variation of post-glacial sediment yield in Chilliwack Valley, British Columbia, *Earth Surf. Processes Landforms*, *36*(2), 229–243, doi:10.1002/esp.2093.
Turowski, J. M., D. Rickenmann, and I. J. Dadson (2010), The partitioning of the total sediment load of a river into suspended load and bedload: A review of empirical data, *Sedimentology*, *57*(4), 1126–1146, doi:10.1111/j.1365-3091.2009.01140.x.
Vinh, V. D., I. Ouillon, T. D. Thanh, and L. V. Chu (2014), Impact of the Hoa Binh Dam (Vietnam) on water and sediment budgets in the Red River basin and delta, *Hydrol. Earth Syst. Sci.*, *18*(10), 3987–4005, doi:10.5194/hess-18-3987-2014.
Walling, D. E. (1983), The sediment delivery problem, *J. Hydrol.*, *65*(1), 209–237.
Walling, D. E. (2008), The changing sediment load of the Mekong River, *Ambio*, *37*(3), 150–157.
Wilcock, P. R. (1993), Critical shear stress of natural sediments, *J. Hydraul. Eng.*, *119*(4), 491–505.
Wilcock, P. R. (1998), Two-fraction model of initial sediment motion in gravel-bed rivers, *Science*, *280*(5362), 410–412, doi:10.1126/science.280.5362.410.
Wilcock, P. R., and J. Crowe (2003), Surface-based transport model for mixed-size sediment, *J. Hydraul. Eng.*, *129*(2), 120–128, doi:10.1061/(ASCE)0733-9429(2003)129:2(120).
Wild, D., and D. Loucks (2014), Managing flow, sediment, and hydropower regimes in the Sre Pok, Se San, and Se Kong Rivers of the Mekong basin, *Water Resour. Res.*, *50*, 5141–5157, doi:10.1002/2014WR015457.
Wilkinson, I. N., I. P. Prosser, and A. O. Hughes (2006), Predicting the distribution of bed material accumulation using river network sediment budgets, *Water Resour. Res.*, *42*, W10419, doi:10.1029/2006WR004958.
Wolman, M. G., and J. P. Miller (1960), Magnitude and frequency of forces in geomorphic processes, *J. Geol.*, *68*(1), 54–74.
Wong, M., and G. Parker (2006), Reanalysis and correction of bed-load relation of Meyer-Peter and Müller using their own database, *J. Hydraul. Eng.*, *132*(11), 1159–1168, doi:10.1061/(ASCE)0733-9429(2006)132:11(1159).
Wu, B., A. Molinas, and A. Shu (2003), Fractional transport of sediment mixtures, *Int. J. Sediment Res.*, *18*(3), 232–247.